sustainability

MDPI

Article

Improved Drought Prediction Using Near Real-Time Climate Forecasts and Simulated Hydrologic Conditions

Hyunwoo Kang and Venkataramana Sridhar *

Department of Biological Systems Engineering, Virginia Polytechnic Institute and State University, Blacksburg, VA 24061, USA; hwkang@vt.edu
* Correspondence: vsri@vt.edu

Received: 20 April 2018; Accepted: 28 May 2018; Published: 30 May 2018

Abstract: Short-term drought forecasting is helpful for establishing drought mitigation plans and for managing risks that often ensue in water resource systems. Additionally, hydrologic modeling using high-resolution spatial and temporal data is used to simulate the land surface water and energy fluxes, including runoff, baseflow, and soil moisture, which are useful for drought forecasting. In this study, the Soil and Water Assessment Tool (SWAT) and Variable Infiltration Capacity (VIC) models are used for short-term drought forecasting in the contiguous United States (CONUS), as many areas in this region are frequently affected by varying drought intensities. Weekly-to-seasonal meteorological inputs are provided by the Climate Prediction Center (CPC) for the retrospective period (January 2012 to July 2017) and Climate Forecasting System version 2 (CFS v2) for the forecasting period (August 2017 to April 2018), and these inputs are used to estimate agricultural and groundwater drought conditions. For drought assessment, three drought indices, namely, the Standardized Soil Moisture index (SSI), the Multivariate Standardized Drought Index (MSDI), and the Standardized Baseflow index (SBI), were analyzed. The accuracy of the forecasting results was verified using several a performance measure (Drought area agreement (%); DA). Generally, eight weeks of lead time forecasting showed good drought predictability from both the SWAT and VIC models for the MSDI simulations (62% for SWAT and 64% for VIC for all drought categories). However, the DA values for eight weeks lead time forecasting for SSI were 23% (SWAT) and 10% (VIC) and 7% (SWAT) and 7% (VIC) for the SBI, respectively. In addition, the accuracies of drought predictions remarkably decreased after eight weeks, and the average DA values were 36% for SWAT and 38% for VIC due to an increase in the uncertainties associated with meteorological variables in CFS v2 products. For example, there are increases in the total number of grids where the absolute values of monthly differences between CFSv2 and CPC observations exceed 20 mm and 1 °C during the forecasting period. Additionally, drought forecasting using only one variable (i.e., SSI and SBI) showed low prediction performances even for the first eight weeks. The results of this study provide insights into drought forecasting methods and provide a better understanding to plan for timely water resource management decisions.

Keywords: drought forecasting; hydrologic models (SWAT and VIC); CFSv2; SSI; MSDI

1. Introduction

Droughts have negatively affected water resource management, agriculture, the environment and the economy around the globe [1,2]. During the last few decades, the severity and frequency of droughts in the United States (U.S.) have been exceptionally high in the West, the Great Lakes States, and the Southeastern U.S. [3,4]. The severity and frequency of recent droughts in the U.S.

coincide with high temperatures and evaporative demand [5], affecting many areas in the contiguous U.S. (CONUS) [6].

An early drought warning framework with short-term drought forecasting (e.g., monthly or seasonal) would provide information regarding the initiation, propagation, and termination of droughts, which are essential for stakeholders and decision-makers [7]. Additionally, seasonal drought forecasting plays a significant role in establishing proper policies to plan for available water resources as well as drought preparedness, mitigation, and risk management. Accurate drought forecast systems would enable optimal operation of irrigation systems by mitigating the detrimental effects of droughts [8]. In recent decades, several drought forecasting systems have evolved to perform the evaluation of hydrologic/drought conditions across the CONUS, such as the Climate Prediction Center's (CPC) Seasonal Drought Outlook [9], the National Integrated Drought Information System's (NIDIS's) Drought Early Warning Systems (DEWS), Princeton University's drought forecast system [10], and a probabilistic drought forecasting framework [11]. Although these studies have proposed some advanced drought forecasting methods, such as probabilistic drought forecasting, the model-based Drought Monitoring and Prediction System (DMAPS) [10], and the dynamical or statistical-dynamical seasonal forecasting [12], the effects of climate change on droughts across various regions of the globe suggests the need for more reliable methods in predicting extreme events because climate change may lead to more extreme hydrometeorological conditions, such as floods or droughts [13,14].

Drought indices are used for evaluating drought levels, drought impacts [15], long-term drought projections, and seasonal drought forecasting [16–19]. Several drought indices have been developed and applied to evaluate multiple categories of drought (e.g., meteorological, agricultural, hydrological, and socio-economic droughts). The Standardized Precipitation Index (SPI) [20] is one of the most widespread indices that is used to evaluate meteorological droughts [21–23], and is used for drought forecasting [24,25]. In the same framework as SPI, the Standardized Soil Moisture Index (SSI) [26,27] is used to quantify agricultural drought conditions. Additionally, the Multivariate Standardized Drought Index (MSDI), which is computed using multiple hydrometeorological variables, is used to identify historic droughts in the U.S. [26,27]. The diverse applications with multiple drought indices allow the consideration of various aspects of drought conditions. In this study, the SSI, MSDI, and Standardized Baseflow Index (SBI) were used, as they represent multiple aspects of drought conditions including agricultural, multivariate, and hydrological droughts in the CONUS.

Drought prediction is commonly based on drought indices, which are estimated using deterministic or statistical model simulations of hydrometeorological variables, such as evapotranspiration, runoff, and soil moisture [17,28]. The SPI was widely used for short-term drought forecasting [24,29,30], and soil moisture-based drought indices were also applied [7,31,32]. Additionally, macro-scale hydrologic models have been employed for the calculation of hydrologic variables based on energy fluxes and water balance estimates, and have been effectively used to assess drought conditions [17,33]. For example, the Variable Infiltration Capacity (VIC) [34] model is a useful tool for simulating hydrologic variables and drought indices [35]. Additionally, the Soil and Water Assessment Tool (SWAT) [36] is an acceptable tool for computing and assessing drought conditions. Thus, hydrological models provide the basis for evaluating drought conditions with multiple drought indices, drought management, and suggesting mitigation strategies for stakeholders [37].

A myriad of studies have evaluated monthly to seasonal forecasting techniques; such investigations were limited to lead times of 1–3 months [38], and a longer lead time drought prediction approach was not available [39]. Hence, a drought forecasting approach with multiple hydrologic models, drought indices, and a longer lead time of meteorological input can facilitate drought preparation, drought mitigation strategies, and drought risk management for the near future. The objectives of this study were to integrate physically based water balance components from the VIC and SWAT models to derive drought indices with short-term meteorological forecasts of precipitation and temperature from the Coupled Forecast System Model version 2 (CFSv2) [40] for near-real-time drought forecasting with lead times up to nine months for the CONUS. To achieve the objective,

the SWAT and VIC models were used to estimate various hydrologic variables including soil moisture, baseflow, and evapotranspiration for both retrospective (January 2012 to July 2017) and forecasting (August 2017 to April 2018) periods. Additionally, multiple drought indices were derived at a weekly time step, and were used to develop weekly forecasts for the CONUS. Finally, an evaluation of drought forecasting with a lead time up to nine months and an assessment of spatial characteristics of droughts were performed by comparing the results to the U.S. Drought Monitor [41,42].

2. Methods

2.1. Study Area

The study area is the CONUS, where drought is an ongoing problem in multiple regions such as the South, West, Central High Plains, and the southeastern regions in the CONUS. Figure 1a shows the entire CONUS and an example map of the USDM for 22 February 2018 that shows current drought conditions. Additionally, Figure 1b,c show the delineated sub-watersheds from the SWAT model (3972 sub-watersheds) and the VIC model grids, respectively. Finally, Figure 1d shows the locations of soil moisture observation from the U.S. Climate Reference Network (USCRN) that were used for interpreting the simulation results.

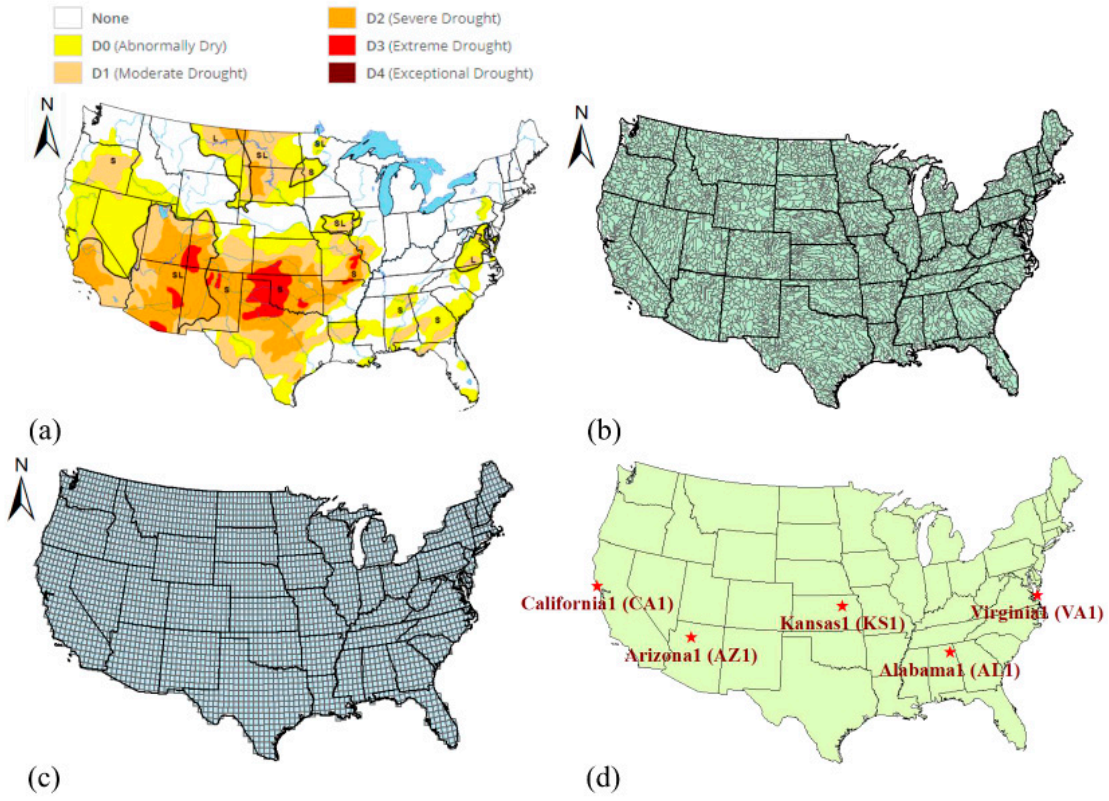

Figure 1. Map of the contiguous United States (CONUS). (**a**) An example map of the United States Drought Monitor (USDM) on 22 February 2018 [41]. (**b**) Entire sub-watersheds delineated by the Soil and Water Assessment Tool (SWAT) model (3972 watersheds). (**c**) Entire grids for the Variable Infiltration Capacity (VIC) model (3275 grids). (**d**) Locations of soil moisture observations from the United States Climate Reference Network (USCRN).

Droughts and heat waves have inflicted damages costing $210.1 billion from 1980–2011 in the U.S., which was ranked the second highest recorded financial losses in the country [43]. Additionally, the 2012–2013 drought caused $40 billion in losses in agricultural areas, and two-thirds of the CONUS was affected [44]. Furthermore, the 2012–2015 California drought was the most severe drought with

a cumulative deficit of precipitation with a 1000-year return period [45,46]. Figure 2 shows drought maps and precipitation and temperature anomalies for the corresponding times for the retrospective period (2012 to 2017). From 2012 to 2015, there was significantly low precipitation or high temperature, which were the primary drivers of droughts. For example, Figure 2a shows the drought conditions of the USDM, the MSDI from SWAT and VIC, and precipitation and temperature anomalies on 8 May 2012. During this time, low precipitation in the west (Nevada, Utah, Arizona, and Colorado) and southeast (Alabama, Georgia, and Florida), and high temperatures were recorded in southwestern areas (California). Accordingly, moderate to severe drought conditions appeared in the regions low precipitation or high temperature. In addition, less precipitation and higher temperatures occurred in the Northern High Plains (Montana, North Dakota, Minnesota, South Dakota, and Nebraska) on 18 July 2017, after which severe to exceptional drought conditions occurred (Figure 2f).

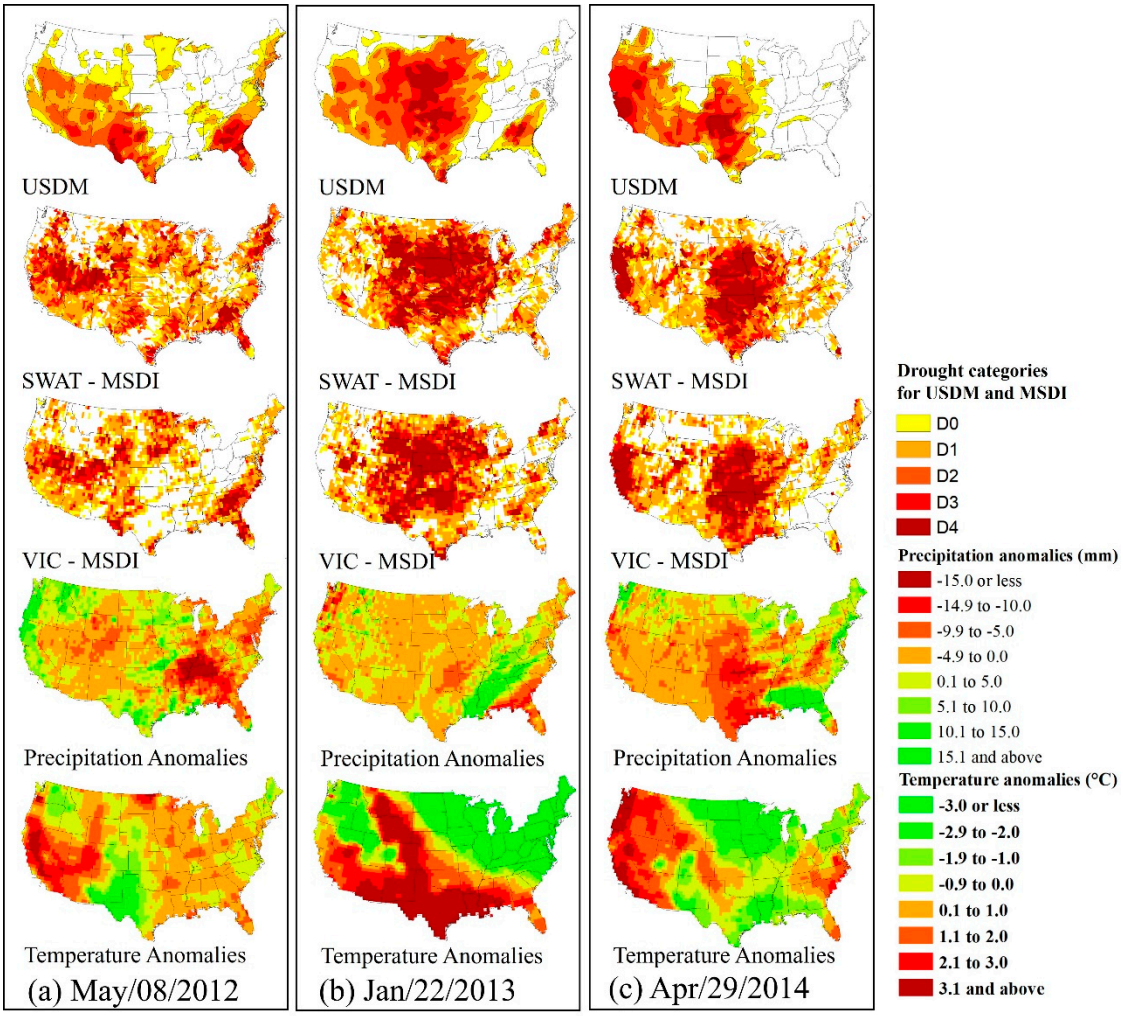

Figure 2. *Cont.*

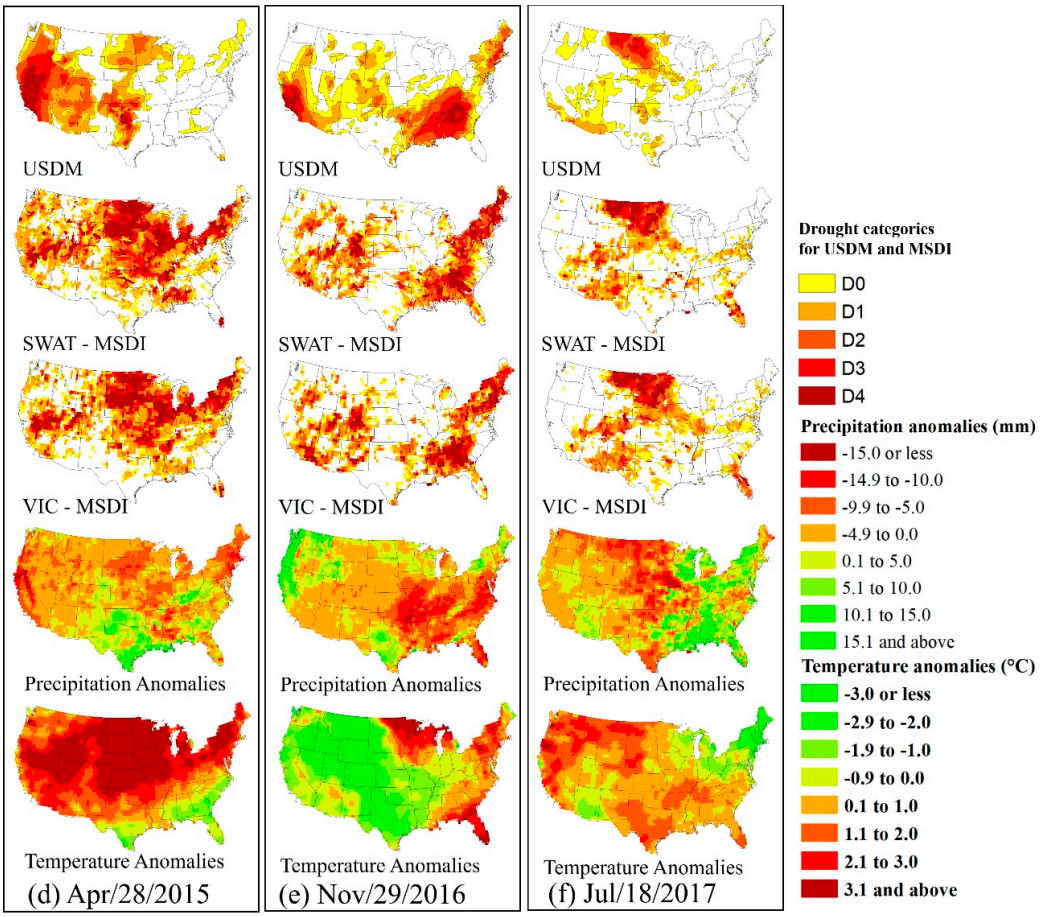

Figure 2. Spatial maps of drought conditions derived from the USDM, MSDI from SWAT and VIC, and precipitation and temperature anomalies for the retrospective period. For the USDM and MSDI maps, yellow to brown areas represent each category of drought conditions. For the maps of precipitation anomalies, orange or red areas indicate less precipitation than mean values, whereas yellowish green or green areas represent more precipitation than mean values. For the maps of temperature anomalies, yellowish green or green areas indicate lower temperatures than mean values, whereas orange or red areas represent higher temperatures than mean values. (**a**) Spatial maps of the USDM and MSDI, precipitation anomalies, and temperature anomalies for 8 May 2012. (**b**) Spatial maps of the USDM and MSDI, precipitation anomalies, and temperature anomalies for 22 January 2013. (**c**) Spatial maps of the USDM, precipitation anomalies, and temperature anomalies for 29 April 2014. (**d**) Spatial maps of the USDM and MSDI, precipitation anomalies, and temperature anomalies for 28 April 2015. (**e**) Spatial maps of the USDM and MSDI, precipitation anomalies, and temperature anomalies for 29 November 2016. (**f**) Spatial maps of the USDM and MSDI, precipitation anomalies, and temperature anomalies for 29 November 2016 (18 July 2017).

2.2. Hydrologic Models and Data

In this study, two hydrologic models were used to estimate several hydrologic variables and drought indices for both retrospective and nine-month lead forecasting of drought conditions. The VIC model [34] is a macro-scale hydrologic model, which has been extensively used to evaluate drought conditions over many river basins in the CONUS and elsewhere to assess retrospective droughts [47,48], to evaluate drought under a future climate [13,49], and to forecast over short-term periods [10,50,51].

The hydrologic estimation of the VIC model depends on the interaction between soil and vegetation layers in each grid cell and forcing variables such as precipitation and temperature. In this study, the VIC model was applied at 0.5-degree resolution with atmospheric forcing from

the Climate Prediction Center's (CPC) global daily precipitation and temperature data [52,53]. CPC precipitation and temperature data were available from 1979 to present (July 2017; 39 years), which was sufficient for simulating long-term hydrologic variables and computing drought indices [54]. Additionally, other model parameters were derived from [55] and [56], and the VIC 4.1.1. version (University of Washington, Seattle, WA, USA)was used due to the comparability with the input dataset. For the CONUS, the VIC model was represented with 3275 grid cells (Figure 1c).

The SWAT model [34,57,58] is a river basin-scale, semi-distributed, and continuous-time model that simulates hydrologic processes in large river basins with mixed land uses and soil types. SWAT is widely used to evaluate drought conditions in many river basins in the U.S. to assess the impacts of climate change on droughts [16,59–61], and drought forecasting [17]. Additionally, SWAT showed higher potential and suitability for drought forecasting at the continental scale [62]. The SWAT model is primarily based on hydrologic response units, which are a specific combination of land use, soil, and slope. Additionally, the model classifies three storage volumes in hydrologic response units (HRUs), which are the unsaturated soil profile layer (0–2 m), the shallow aquifer (2–20 m), and the deep aquifer (>20 m). The SWAT model simulates infiltration, surface runoff, lateral flow, shallow and deep aquifers baseflow, and evapotranspiration. The SWAT model requires a digital elevation model (DEM), soil, and meteorological input, such as precipitation and temperature. In this study, a 30 arc-second DEM from the U.S. Geological Survey [63] was used, a soil map with a 1:250,000 scale was obtained from State Soil Geographic data (STATSGO) [64], and a land use map was obtained from National Land Cover Data (NLCD) [65]. In this study, 3973 sub-watersheds were delineated using the SWAT model to consider all of the climate grid cells in the CONUS.

The retrospective simulation periods for both the VIC and SWAT models were 1979 to July 2017 with input data for 30 years [54]. Additionally, the period from January 2012 to July 2017 was selected for the evaluation of drought areas because continuous and diverse severities of drought conditions occurred over the CONUS during this period [66,67].

For the historic simulation, 0.5 degree resolution data of daily precipitation and temperature were obtained from the CPC Global Unified precipitation and temperature database [52,53]. The CPC provides 0.5 degree resolution precipitation rate (unit: $kg/m^2/s$) and temperature (unit: K) data at the global scale in a NetCDF format. These variables were transformed into daily precipitation (unit: mm) and temperature (unit: °C) data that were then used as inputs for both the SWAT and VIC models. For the forecasting simulation analysis, forecast variables up to nine months into the future were also transformed and used for future simulation including CFSv2 precipitation rate (unit: $kg/m^2/s$) and temperature (unit: K) data .

2.3. CFSv2

The Coupled Forecast System Model version 2 (CFSv2) uses real-time data to compute atmospheric variables with a lead time up to nine months, including four-time initializations a day. Additionally, CFSv2 consists of a spectral atmospheric model (Global Forecast System; GFS) at a T126 (approximately 0.937°) resolution with 64 hybrid vertical levels and the advanced version of the ocean model [68]. Precipitation and temperature data were obtained from the CFSv2 data for the period between August 2017 and April 2018. Since the spatial resolution of CFSv2 is T126 (approximately 0.937°), it should be downscaled to 0.5 degree for the SWAT and VIC models. Thus, kriging, a spatial interpolation method, was applied to the downscaling process for each day of forecasting (August 2017 to April 2018). Additionally, mean values of precipitation and temperature data from the four initialization (00, 06, 12, and 18 h) for 1 August 2017 were used. To remove the bias from the forecast data, a bias correction was performed by adding or subtracting the difference in weekly accumulated CFSv2 precipitation for each climate grid with reference to the CPC dataset (1979 to 2017). Figure 3a shows the time series of weekly raw and bias-corrected precipitation for the entire CONUS, and there is an overall overestimation of precipitation from the CFSv2 raw data. Additionally, Figure 3b shows the spatial map of precipitation differences between raw and bias-corrected data, and the

overestimated precipitation from CFSv2 raw data was evident for the entire domain, specifically the eastern and west coast regions. Figure 3c,d show the time series and spatial map of temperature differences between the raw and bias-corrected data, and there is an overestimation in the western areas of the CONUS, as well as an underestimation in the Northern High Plains.

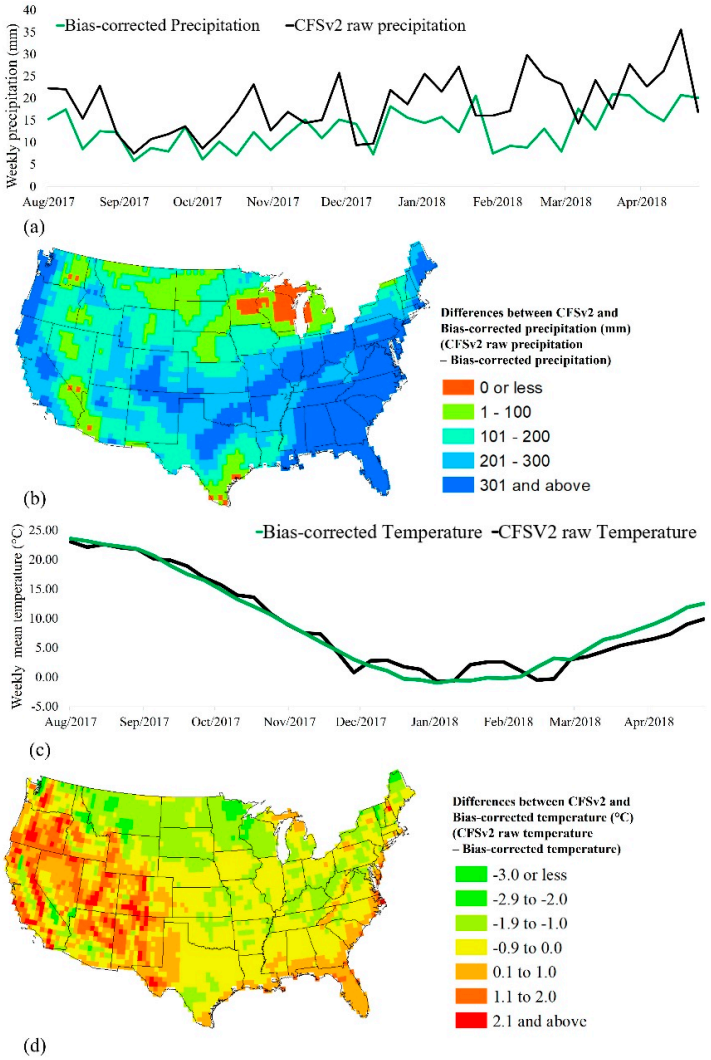

Figure 3. Comparisons of raw and bias-corrected precipitation and temperature from the CFSv2 dataset. (**a**) Time series for weekly precipitation from raw (black line) and bias-corrected (green) data for the CONUS. The *X*-axis represents the forecasting period, and the *Y*-axis shows weekly precipitation. (**b**) Spatial map of differences between raw and bias-corrected precipitation during the forecasting period (August 2017 to April 2018). Positive values indicate that higher precipitation was estimated by CFSv2 compared to the mean values of historic observations (1979 to July 2017), and they are symbolized as light blue to blue. Negative values indicate that less precipitation was estimated by CFSv2, and they are symbolized as red. (**c**) Time-series for weekly mean temperature from raw (black line) and bias-corrected (green) data for the CONUS. The *X*-axis represents the forecasting period, and the *Y*-axis shows weekly mean temperature. (**d**) Spatial map of differences between raw and bias-corrected temperature during the forecasting period (August 2017 to April 2018). Positive values indicate that a higher temperature was estimated by CFSv2 compared to the mean values of historic observations (1979 to July 2017), and they are symbolized as orange to red. Negative values indicate that a lower temperature was estimated by CFSv2, and they are symbolized as yellowish green to green.

2.4. USDM and Drought Categories

The USDM is the most representative drought indicator in the U.S. and this indicator produces a weekly map of drought conditions in collaboration with the U.S. Department of Agriculture (USDA), the National Drought Mitigation Center (NDMC), and the National Oceanic and Atmospheric Administration (NOAA) [41]. The USDM is a composite index that includes many indicators (e.g., Palmer Drought Severity Index, SPI, Keetch-Byram Drought Index, modeled soil moisture, seven-day average streamflow, precipitation anomalies, and satellite vegetation health), climate indices, and local reports from more than 350 expert observers across the entire U.S. Additionally, the USDM provides a weekly map of drought with five drought categories, and is classified based on a percentile approach (Table 1). Furthermore, the USDM can identify both short and long-term drought conditions, and it provides consistent drought conditions in the U.S.

Table 1. Descriptions of drought categories associated with the USDM and drought indices derived from the two models used in this study.

USDM Category	Description	Range of Drought Indices
D0	Abnormally dry	−0.50 to −0.79
D1	Moderate drought	−0.80 to −1.29
D2	Severe drought	−1.30 to −1.59
D3	Extreme drought	−1.60 to −1.99
D4	Exceptional drought	−2.0 or less

2.5. Drought Indices

In this study, the VIC and SWAT models were used to estimate the input variables of several drought indices such as the Standardized Soil Moisture Index (SSI), the Standardized Baseflow Index (SBI), and the Multivariate Standardized Drought Index (MSDI) to assess the historic and forecasted drought conditions in the CONUS. For example, model-estimated baseflow was used to compute SBI, and soil moisture was used to calculate the SSI and MSDI.

The computation of multivariate drought indices included using joint probability and distribution models [16,26,69], and the MSDI was computed using the joint probability of long-term precipitation and soil moisture records [26,70]. The joint distribution of two variables is described as:

$$P(X \leq x,\ Y \leq y) = p \tag{1}$$

where p is the joint probability of the precipitation and soil moisture. Additionally, the MSDI can be computed as follows [26]:

$$\text{MSDI} = \varnothing^{-1}(p) \tag{2}$$

where $\varnothing$ is the standard normal distribution function.

In this study, the Gringorten plotting position formula, which is an alternative calculation that can be used to compute empirical joint probability, was used [70,71] and is defined as follows:

$$P(x_k, y_k) = \frac{m_k - 0.44}{n + 0.12} \tag{3}$$

where m_k is the number of occurrences of the pair (x_i, y_i) for $x_i \leq x_k$ and $y_i \leq y_k$, and n is the number of the observations. To compute SSI and SBI, the univariate form of the Gringorten plotting formula (Equation (4)) [70] was used and is defined as follows:

$$P(x_i) = \frac{i - 0.44}{n + 0.12} \tag{4}$$

where n is the number of observations and i is the rank of the observed values from the smallest to the largest. The weekly scales of SSI, SBI, and MSDI (25-week scale) were computed using the input and output variables from the VIC and SWAT models, and were subsequently used to evaluate historic and forecasted drought conditions in the CONUS.

3. Results and Discussion

3.1. Validation of Retrospective Drought Conditions with USDM (Drought Agreement Area)

3.1.1. Comparisons to USDM Drought Maps of Drought Areas

The drought severity maps from the drought indices and the two models were compared with the respective USDM drought severity maps to evaluate the accuracy of the drought indices. Figure 4 provides comparisons of the drought indices from two models and the USDM severity areas for the retrospective period, which is from January 2012 to July 2017. Since the USDM drought areas were estimated based on a weekly time step, the three drought indices (MSDI, SSI, SBI) were calculated at the same temporal scale for the corresponding dates with USDM. Overall, the total drought area for the CONUS region decreased in the retrospective period, and the overall trend of drought areas was captured by the drought indices from the two models.

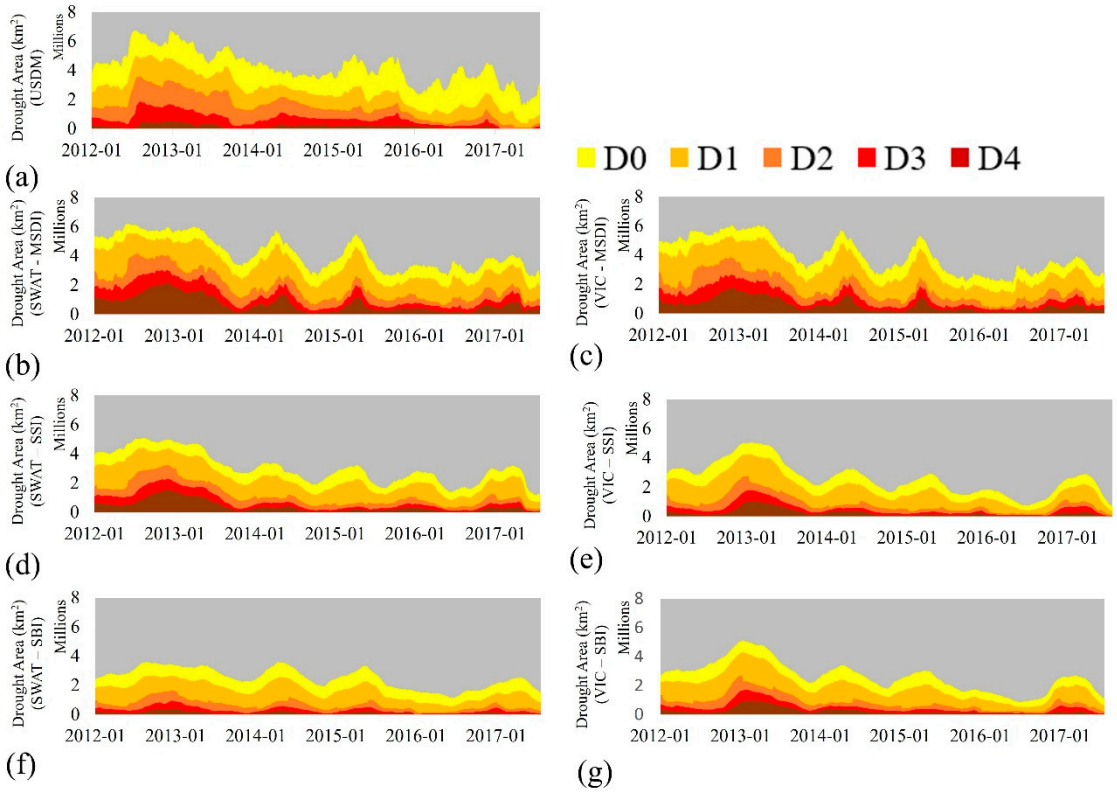

Figure 4. Weekly comparisons of drought areas of the United States Drought Monitor (USDM) and drought indices computed from the Variable Infiltration Capacity (VIC) and Soil and Water Assessment Tool (SWAT) models for the period between 2012 and 2017. (**a**) Weekly drought categories from the USDM. (**b**) Weekly drought categories from the results of the SWAT model and MSDI. (**c**) Weekly drought categories from the results of the VIC model and MSDI. (**d**) Weekly drought categories from the results of the SWAT model and SSI. (**e**) Weekly drought categories from the results of the VIC model and SSI. (**f**) Weekly drought categories from the results of the SWAT model and SBI. (**g**) Weekly drought categories from the results of the VIC model and SBI.

For the results of MSDI, mean values of total drought area (D0 to D4 categories) were 4.22 million km^2 and 3.95 million km^2 for the SWAT and VIC models, respectively. Additionally, mean values of the total drought area were 3.06 million km^2 and 2.61 million km^2 for the SSI simulation and 2.51 million km^2 and 2.65 million km^2 for the SBI simulation. Overall, the MSDI simulations estimated more drought areas than other drought indices, and the SWAT model simulated larger drought areas except for the results of SBI. Figure 5 shows the mean values of MSDI, SSI, SPI, and QQ, which is the sum of surface runoff and baseflow for the entire CONUS during the retrospective period, and Figure 5a,b show the results of the SWAT and VIC models, respectively. QQ was calculated as the sum of the surface runoff and baseflow, and SPI was computed using precipitation and Equation (4). The same approach was employed with SSI and SBI. As shown in Figure 5, the mean values of MSDI, SSI, SBI, and SPI were −0.70, −0.37, −0.27, and −0.06 for the SWAT model and were −0.49, −0.08, −0.08, and −0.06 for the VIC model. The results of SPI were similar because it used the same precipitation input (CPC precipitation data). However, the mean values of MSDI and SSI from the SWAT model were lower than those from the VIC model, which indicated higher drought severities and larger drought areas from the SWAT model. These results occurred because of the differences in the estimation of runoff between these two models. For instance, the SWAT model used the Soil Conservation Service (SCS) curve number (CN) [64] and the VIC model used the variable infiltration curve method [72]. For example, SPI values continuously increased during January 2016, and there was a sudden increase in QQ values from the SWAT model (red circled zone). Due to the impact of the peak QQ, the SSI values (orange line) did not follow the SPI values since a higher QQ resulted in lower soil moisture. However, the QQ values from the VIC model at the same time were relatively low, and SSI values followed the SPI. Thus, these results imply that different runoff estimation methods led to differences in simulated soil moisture, and they ultimately impact the results of drought indices and drought assessments. Specifically, the higher sensitivity of the SCS CN method in the SWAT model appeared to cause these discrepancies [73].

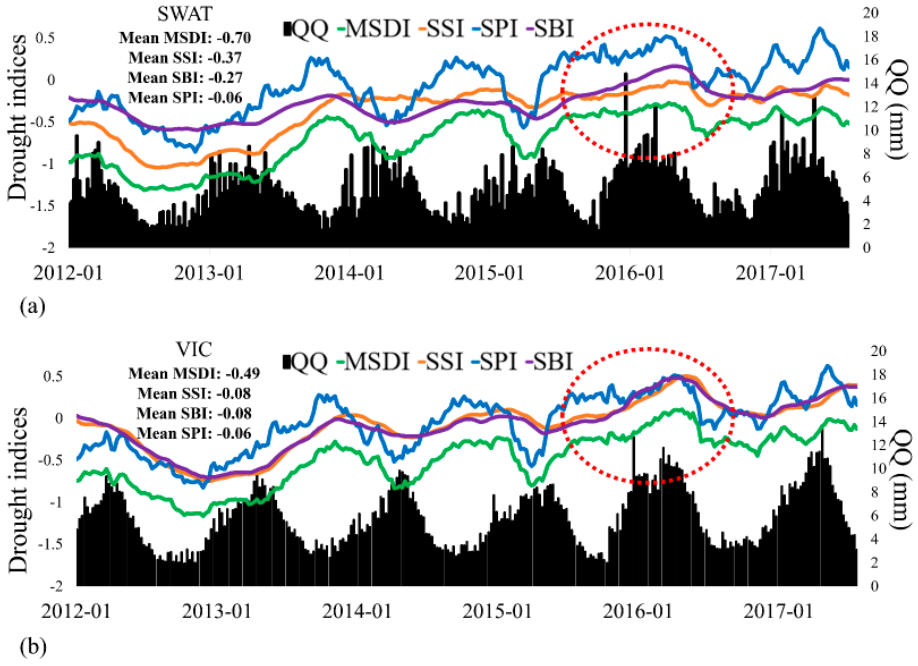

Figure 5. Time-series of mean values of MSDI, SSI, SBI, SPI, and QQ for the CONUS during the retrospective period. Each line indicates the drought index (green: MSDI, orange: SSI, violet: SBI, Blue: SSI), and they are represented by the primary *Y*-axis (left). Black bars show the QQ values, and they are represented by the secondary *Y*-axis (right). (**a**) Results of the SWAT model. (**b**) Results of the VIC model.

Figure 6 shows the values of the drought agreement (DA) area for each drought index. DA was calculated as a rate of intersected areas where drought severities were correctly captured per total area of the USDM. Additionally, Table 2 provides the mean values of DA for the drought indices during the retrospective period. Overall, the performances of the VIC model were slightly higher than those of the SWAT model from all the three drought indices, and it was also affected by the different methods water budget estimation associated with the SWAT and VIC models. Additionally, the retrospective period (2012 to 2017) was the time that the second lowest precipitation (six-year mean) was recorded in the last 30 years in the CONUS (Table 3). The SWAT model responded more sensitively than the VIC model, which was represented by the lower mean values of the drought indices (e.g., MSDI and SSI) (Figure 5).

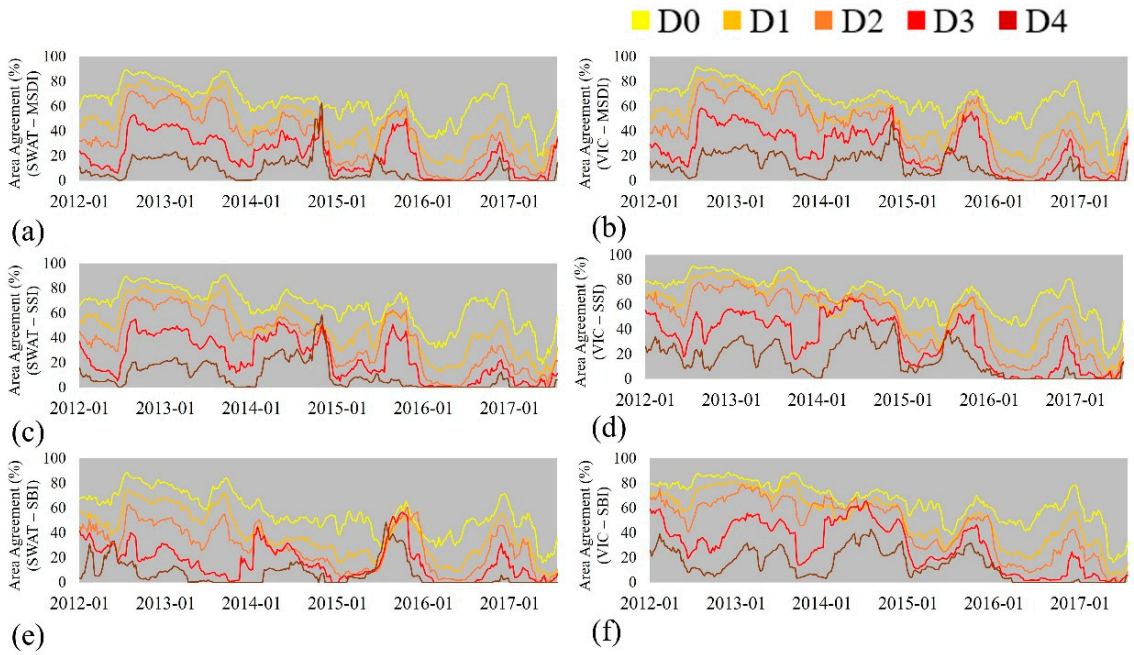

Figure 6. Weekly time-series of drought agreement (DA) values for each drought category from the two models. The DA was calculated as the ratio of the intersected area to the total area of the USDM (Intersected area/USDM area). (**a**) DA values of MSDI from the SWAT model. (**b**) DA values of MSDI from the VIC model. (**c**) DA values of SSI from the SWAT model. (**d**) DA values of SSI from the VIC model. (**e**) DA values of SBI from the SWAT model. (**f**) DA values of SBI from the VIC model.

Table 2. Mean drought agreement (DA) values for three drought indices from the SWAT and VIC models during the retrospective period (January 2012 to July 2017) (unit: %).

Model	Drought Indices	D0	D1	D2	D3	D4
SWAT-DA	MSDI	63	45	35	21	9
	SSI	65	48	37	23	9
	SBI	55	38	28	16	7
VIC-DA	MSDI	66	49	41	26	12
	SSI	67	54	47	30	15
	SBI	65	51	44	28	14

Table 3. Annual precipitation and six years' mean precipitation for the CONUS during last 36 years (unit: mm).

Years	Annual Precipitation	Six Years Mean (1982–1983)	Years	Annual Precipitation	Six Years Mean (1988–1993)	Years	Annual Precipitation	Six Years Mean (1994–1999)
1982	848	795	1988	653	770	1994	771	800
1983	869		1989	730		1995	826	
1984	784		1990	812		1996	858	
1985	750		1991	816		1997	798	
1986	793		1992	792		1998	847	
1987	729		1993	819		1999	699	
Years	**Annual Precipitation**	**Six Years Mean (2000–2005)**	**Years**	**Annual Precipitation**	**Six Years Mean (2006–2011)**	**Years**	**Annual Precipitation**	**Six Years Mean (1982–1983)**
2000	686	726	2006	727	765	2012	671	754
2001	699		2007	734		2013	746	
2002	699		2008	789		2014	750	
2003	735		2009	808		2015	825	
2004	810		2010	789		2016	771	
2005	730		2011	741		2017	759	

The DA values of MSDI, SSI, and SBI from the VIC model (66%, 67%, and 65%) and MSDI and SSI from the SWAT model (63% and 65%) were similar, but the accuracy of SBI from the SWAT model was different (55%). In the case of the VIC model, the trends of drought areas (Figure 4) and the time series (Figure 5) of SSI and SBI were analogous, which indicated that soil moisture and baseflow responded comparably under the same hydro-climatologic conditions (e.g., precipitation and temperature). However, the performances of SSI and SBI from the SWAT model were not comparable due to the fluctuation in runoff estimations.

In the case of extreme or exceptional drought conditions (D3 or D4), drought areas were partially captured by drought indices, which indicated that drought indices overstated the drought severity. This was mainly because the period of climatology for the drought indices (39 years) was shorter than that of the USDM, which contained a much longer record of ground-based observations [27,41]. Additionally, the drought indices were based solely on precipitation, soil moisture, and baseflow conditions, whereas the USDM combined various input variables, even including subjective inputs from local climatologists [41].

The dataset for the VIC model [56] was calibrated by the previous study [5]. Additionally, the SWAT model was not calibrated, but there were no significant differences between the calibrated VIC and uncalibrated SWAT model for the drought estimation during the retrospective period. The main intent was to evaluate how each of these two models was able to perform in capturing the drought and, interestingly, it was found that the results of uncalibrated model are valid for the CONUS region.

3.1.2. Discussions of Drought Categories and USCRN Observation Sites

Figure 7 shows comparisons of soil moisture percentiles from the U.S. Climate Reference Network (USCRN), weekly precipitation and temperature, and USDM drought categories at several sites in the California (CA1), Arizona (AZ1), Kansas (KS1), Alabama (AL1), and Virginia (VA1). Extreme to exceptional drought events (D3 to D4 category) from the results of soil moisture percentile are highlighted by blue boxes, and weekly precipitation and temperature and USDM categories at the corresponding times are highlighted by red boxes. Additionally, Table 4 shows some properties of the USCRN sites. These five sites were selected because various drought severities occurred during the retrospective period, and long-term soil moisture observations were available for these locations. As shown in Figure 7, extreme to exceptional drought events normally occurred under conditions of lower precipitation and higher temperature. However, even though the weekly soil moisture percentile was less than 2% (standard of D4; Table 1), it was not commonly judged as D4 by the USDM for these five sites. However, in the case of other drought categories and total drought events, more drought events occurred at the three sites (AZ1, KS1, and AL1 sites) (Figure 8). Thus, it can be inferred that the USDM maps were usually conservative in designating the exceptional drought conditions (D4), which was the reason that DA values for extreme drought conditions were lower than the abnormal or moderate drought.

Table 4. Some properties of United States Climate Reference Network (USCRN) sites.

Site Name	USCRN Code	Longitude	Latitude	Observation Period
CA1	CA_Fallbrook_5_NE	−123.07	38.32	September 2011—Current
AZ1	AZ_Yuma_27_ENE	−112.34	35.76	August 2009—Current
KS1	KS_Manhattan_6_SSW	−96.61	39.1	August 2009—Current
AL1	AL_Selma_13_WNW	−85.96	34.29	June 2009—Current
VA1	VA_Cape_Charles_5_ENE	−75.93	37.29	June 2011—Current

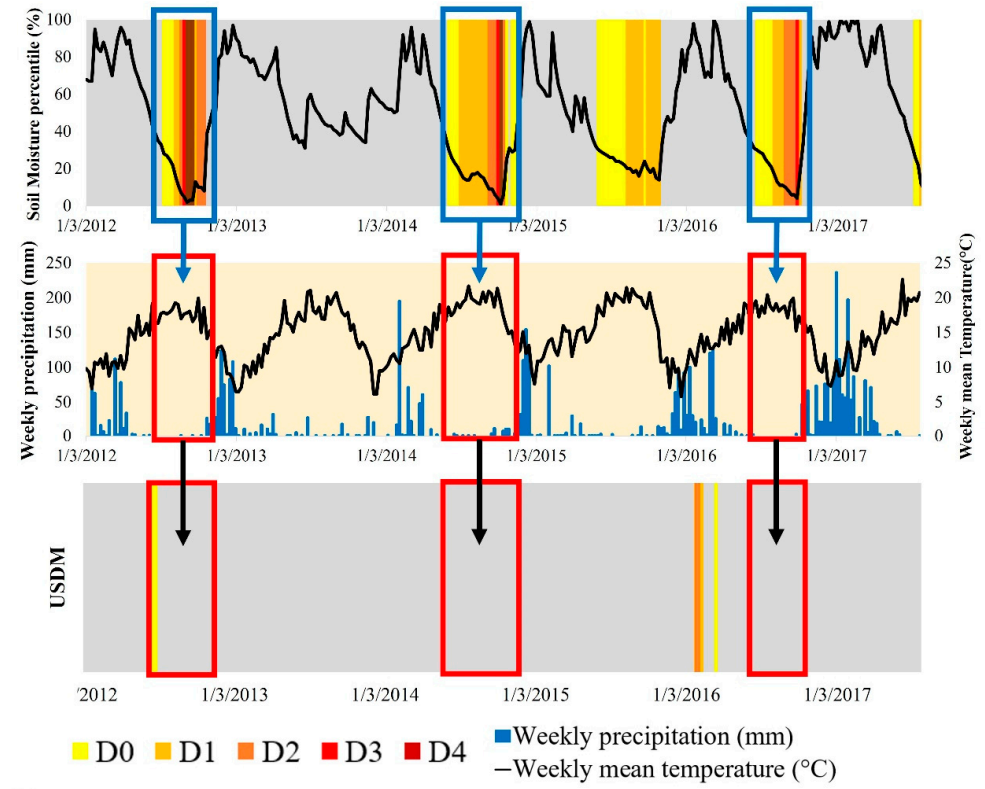

(a)

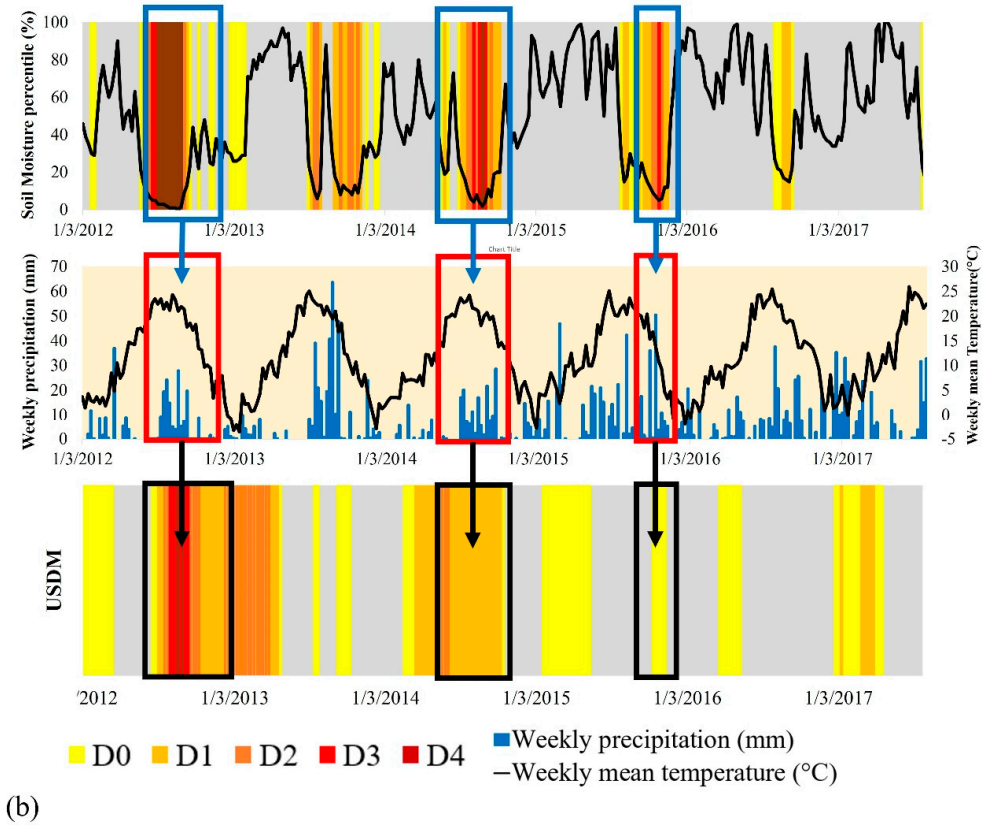

(b)

Figure 7. *Cont.*

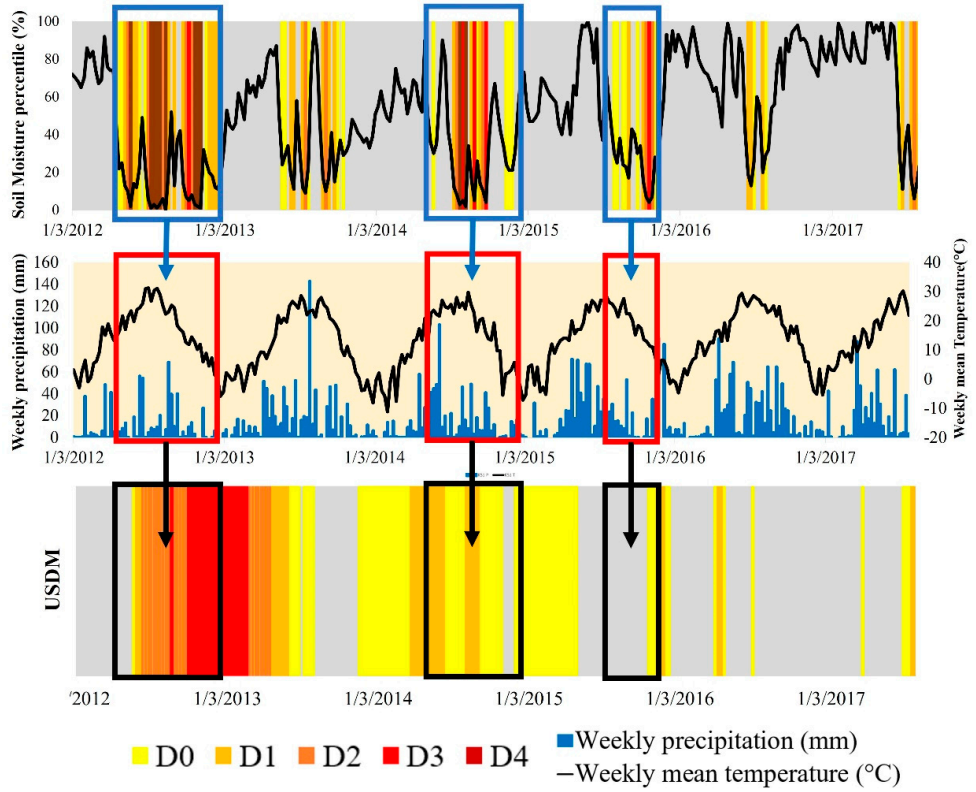

(c)

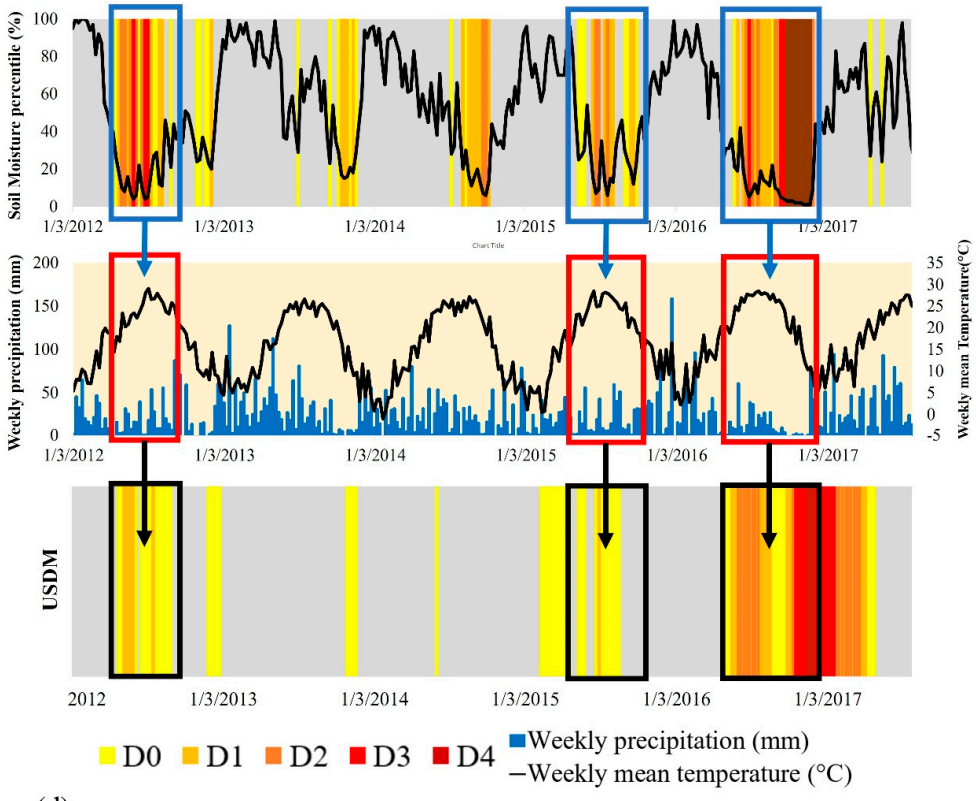

(d)

Figure 7. *Cont.*

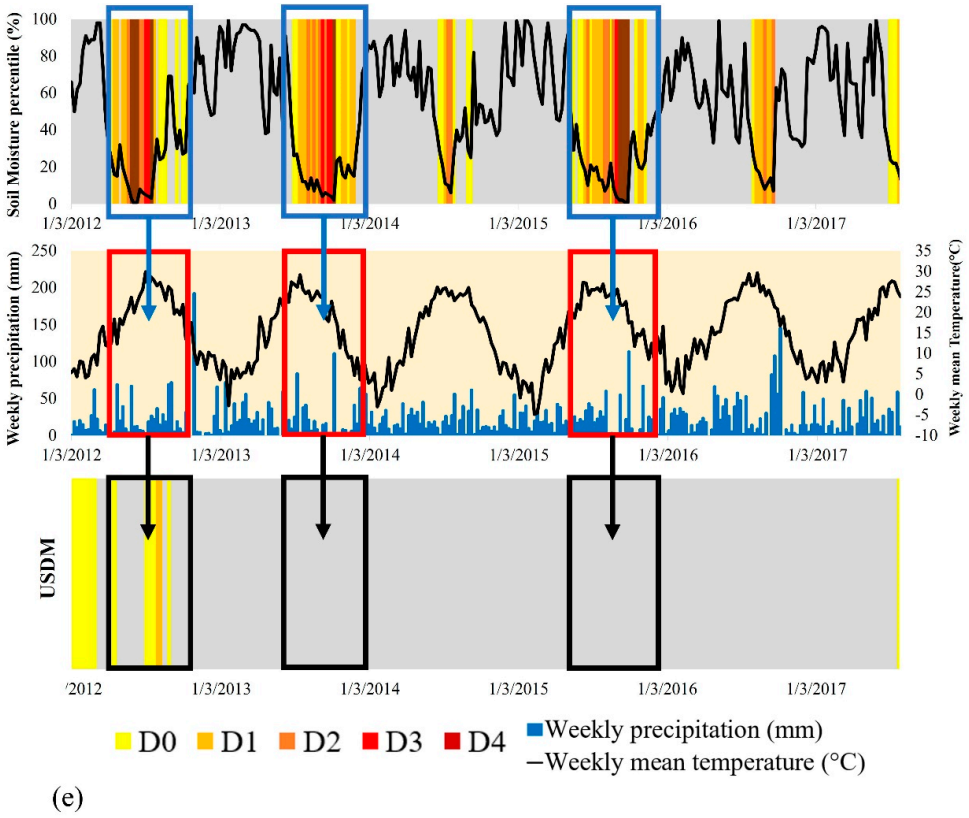

Figure 7. Time series and color maps of soil moisture percentile (first figure), time series of weekly precipitation and temperature (second map), and color map of the USDM (third figure) at the USCRN observation sites for the retrospective period. For the first map, the black line indicates the time-series of soil moisture percentile, and yellow to brown bars represent drought categories. For the second figure, the black line represents the time-series of the weekly mean temperature (°C), and the blue bars indicate the weekly precipitation (mm). For the third figure, the yellow to brown bars represent the drought categories. All boxes represent a period of drought events that includes the D3 or D4 drought category based on soil moisture percentiles (red or brown). (**a**) Results from the CA1 site. (**b**) Results from the AZ1 site. (**c**) Results from the KS1 site. (**d**) Results from the AL1 site. (**e**) Results from the VA1 site.

3.1.3. Comparisons with USDM Drought Maps (Drought Occurrence-Based)

In this study, model-estimated drought occurrences were evaluated by comparisons with weekly USDM maps for the retrospective period (January 2012 to July 2017), and two performance matrices were used. The matrices are:

(a) Index of agreement (IA, Unit: %): Percent of drought occurrences that correctly captured a drought severity of USDM for the total weeks in the watershed.
(b) Index of disagreement (ID, Unit: %): Percent of drought occurrences that failed to capture a drought severity of USDM for the total weeks in the watershed.

Figure 9 shows a classification of Hydrologic Unit Code 6 (HUC6) watersheds for which IA and ID were estimated. All of the HUC6 watersheds in the CONUS were divided into twelve groups, and each group was assigned a number from one to twelve. Each sub-watershed from the VIC and SWAT models was aggregated to HUC6 resolution, and the *X*-axis of Figure 9 represents the code numbers of HUC6. As shown in Figure 9, high numbers represent southwestern regions, whereas low numbers indicate northeastern regions in the CONUS. Additionally, Figures 10 and 11 show the IA and ID assessments of MSDI from the two models for five drought severities including

abnormal (D0 and drought indices < −0.5), moderate (D1 and drought indices < −0.8), severe (D2 and drought indices < −1.3), extreme (D4 and drought indices < −1.6), and exceptional drought conditions (D4 and drought indices < −2.0). The categorization of drought severities provides a relative accuracy of the drought indices in capturing the USDM of a given severity.

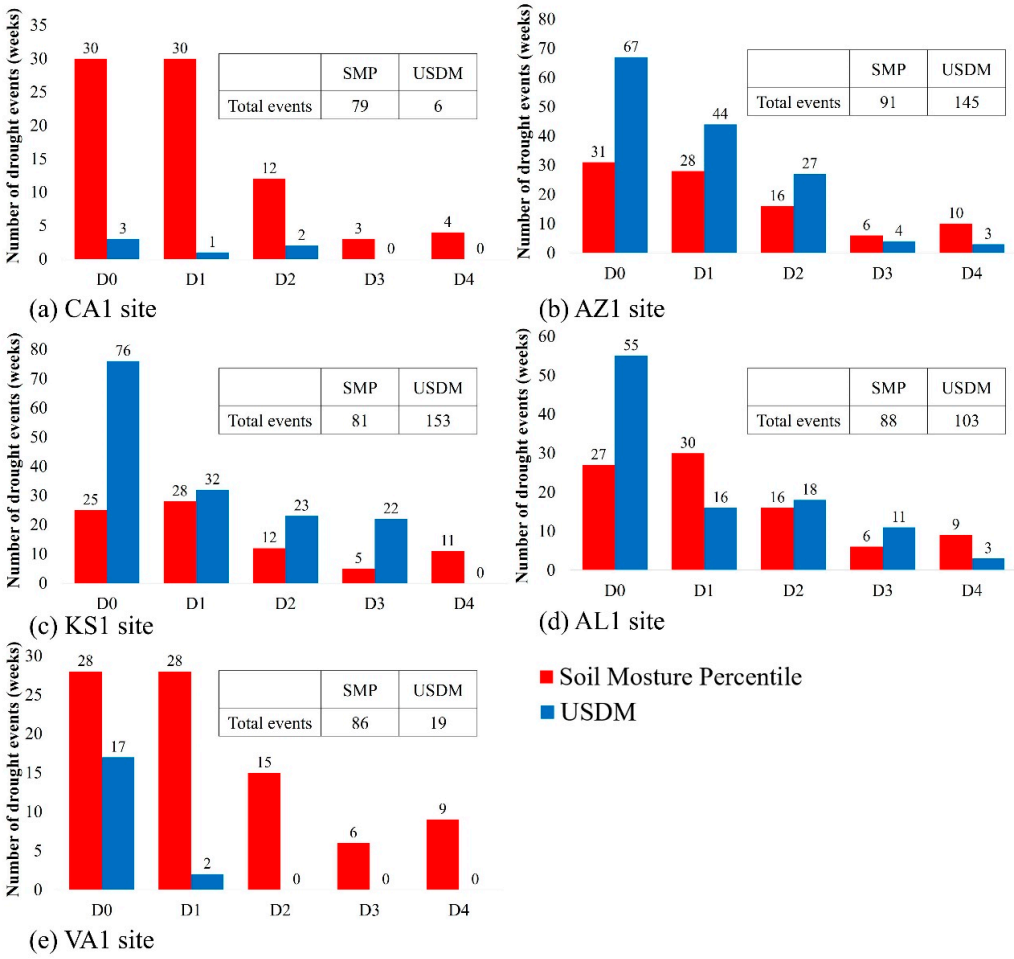

Figure 8. Bar charts and attached tables for drought events (all drought categories) based on soil moisture percentile (SMP) and USDM at USCRN observation sites. The *Y*-axis represents the number of drought events (weeks) and the *X*-axis indicates each drought category. The red bars represent drought events based on the soil moisture percentile, whereas blue bars indicate drought events based on the USDM. The attached tables shows the total number of drought events. (**a**) The CA1 site. (**b**) The AZ1 site. (**c**) The KS1 site. (**d**) The AL1 site. (**e**) The VA1 site.

The results of IA and ID from MSDI and SSI estimation from two models indicate that the mean values of IA were found to be approximately 70% for D0 category (Table 5) for both the SWAT and VIC models, and the results of the two models were similar. Overall, the IA values in the central to southwestern regions were normally higher than in the northeastern areas. Figure 12a,b show the total drought occurrences suggested by the USDM and annual precipitation during the retrospective period (January 2012 to July 2017, 291 weeks). The amount of precipitation was understandably low in areas where a higher number of droughts occurred, and certain areas were affected by droughts for the entire period (e.g., California). Additionally, it was found that the ID values were higher in areas with high precipitation, and there was a linear relationship between annual precipitation and ID values. The correlation coefficient obtained from Pearson's correlation test was 0.54 (p-value < 0.05), and the R^2 value was 0.29 (p-value < 0.05) with a 95% of confidence interval (Figure 12c).

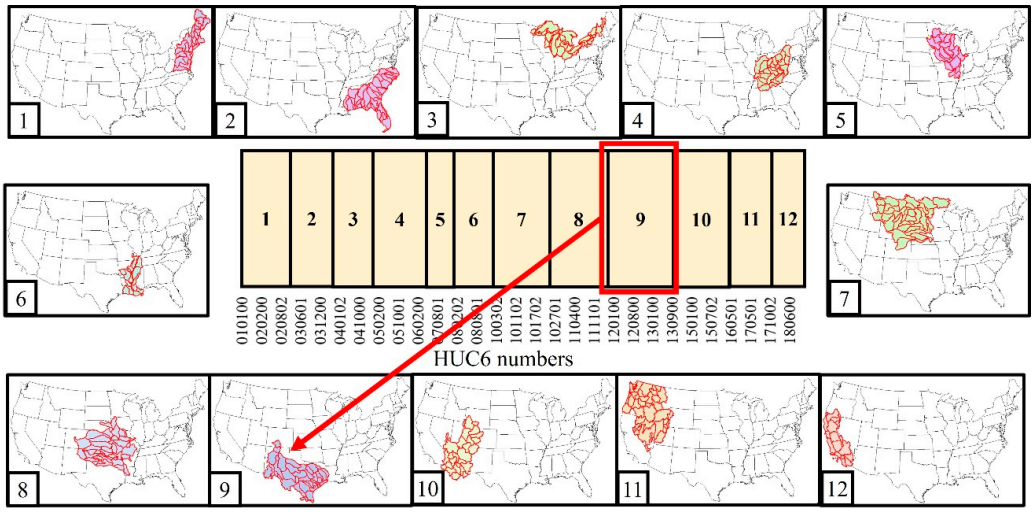

Figure 9. Classification of Hydrologic Unit Code 6 (HUC6) watersheds. The *X*-axis represents the code numbers of HUC6. All of the HUC6 watersheds in the CONUS were classified into twelve groups, and each group was assigned a number from one to twelve. For example, HUC6 watersheds starting with the numbers "12" and "13" were assigned to group number "9", which is highlighted with the red box and arrow.

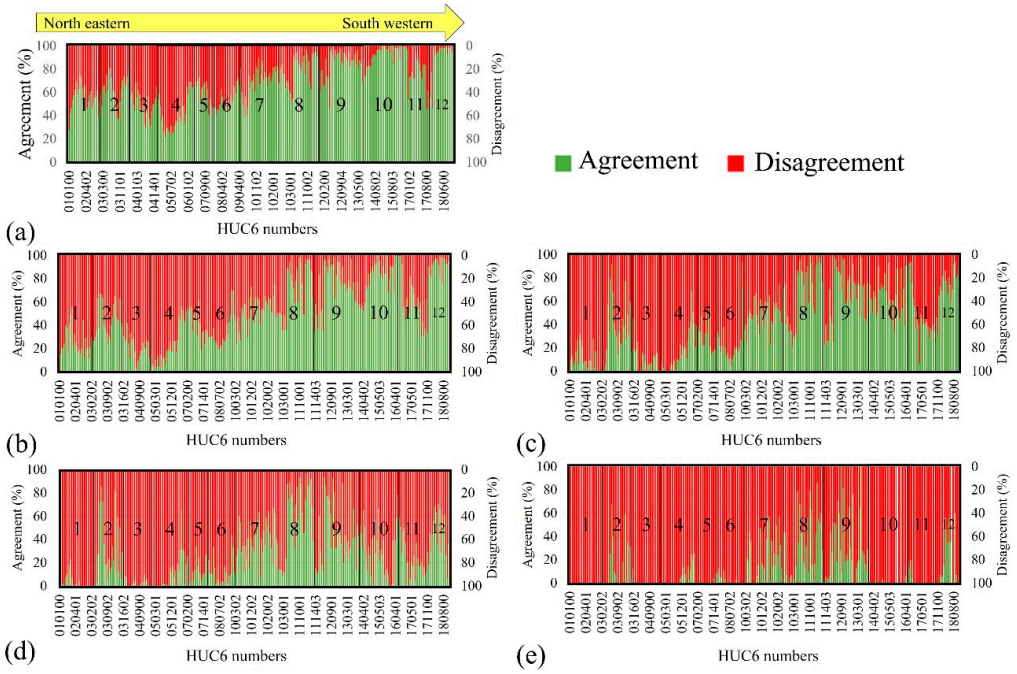

Figure 10. Results of drought occurrence evaluations for all HUC6 watersheds for the CONUS (317 sub-watersheds): Index of agreement (IA) and index of disagreement (ID) between the USDM and MSDI from the SWAT model for five drought categories during the retrospective period (January 2012 through July 2017). The *Y*-axis on the left (primary axis) represents the values of agreement, whereas the *Y*-axis on the right (secondary axis) indicates the values of disagreement. The *X*-axis shows the HUC6 numbers, which were classified into twelve groups (Figure 8). (**a**) Results of D0. (**b**) Results of D1. (**c**) Results of D02 (**d**) Results of D3. (**e**) Results of D4.

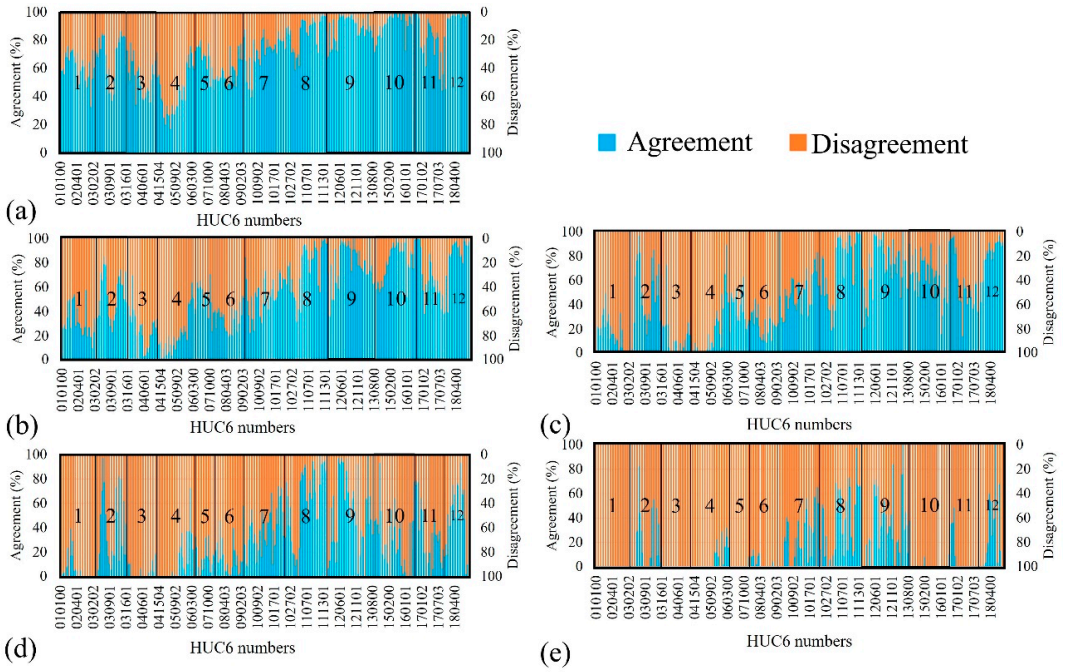

Figure 11. Results of drought occurrence evaluations for all HUC6 watersheds for the CONUS (317 sub-watersheds): Index of agreement (IA) and index of disagreement (ID) between the USDM and MSDI from the VIC model for five drought categories during the retrospective period (January 2012 through July 2017). The *Y*-axis on the left (primary axis) represents the values of agreement, whereas the *Y*-axis on the right (secondary axis) indicates the values of disagreement. The *X*-axis shows the HUC6 numbers, which were classified into twelve groups (Figure 8). (**a**) Results of D0. (**b**) Results of D1. (**c**) Results of D02 (**d**) Results of D3. (**e**) Results of D4.

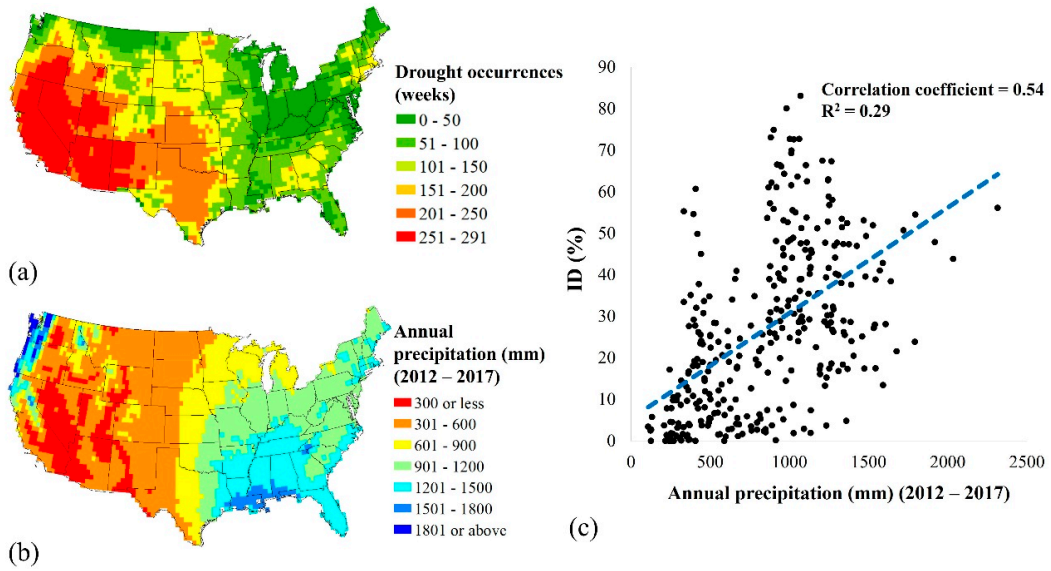

Figure 12. Spatial maps of drought occurrences (unit: weeks) and annual precipitation (unit: mm) during the retrospective period (291 weeks), as well as a scatter plot that shows a relationship between annual precipitation and the index of disagreement (ID). (**a**) Spatial map of drought occurrences. Red areas indicate locations where more droughts occurred, whereas green areas represent regions with fewer droughts. (**b**) Spatial map of annual precipitation. Red areas indicate locations with lower precipitation, whereas blue areas represent regions with higher precipitation. (**c**) Scatter plot. The *Y*-axis represents the ID (%) and the *X*-axis shows the annual precipitation (mm).

Table 5. Mean values of index of agreement (IA) values for drought indices from the SWAT and VIC models (unit: %).

Model	Drought Indices	D0	D1	D2	D3	D4
SWAT	MSDI	70	53	43	28	12
	SSI	71	56	46	29	12
	SBI	64	48	37	21	7
VIC	MSDI	72	56	48	32	13
	SSI	74	60	52	35	17
	SBI	71	56	47	28	12

In addition, the results indicated that the performances of MSDI were the worst in Region 4 (Ohio River Valley), Region 1 (New England), Region 3 (Great Lakes), and Region 2 (Southeastern U.S.) where drought occurrences were low and annual precipitation was high. This was because the drought indices used in this study were based on the empirical probabilistic method, and they were calculated from a relative comparison of a specific week in each year [27]. Thus, even if the actual precipitation was higher than in other regions (e.g., Region 4), it would be declared as a drought-hit area when the precipitation at a certain time was lower than the mean precipitation.

3.2. Evaluation of Drought Forecasting with Weekly Maps of USDM

In this study, seasonal drought forecasts leading up to nine months into the future using two hydrologic models and the CFSv2 meteorological dataset were developed and analyzed, and forecasted drought areas from drought indices were evaluated with USDM maps. The forecasting period was August 2017 to April 2018, but the drought area evaluation with USDM maps was performed during August 2017 to January 2018, which was expected to serve as a hindcast validation. After July 2017, an increase in drought areas was reported by the USDM (Figure 13a) over a period of six months, and results of all drought indices showed an increase in total drought areas. Compared to the last week of July 2017, there was a 2% increase in the first week of October, a 48% increase in the third week of December, and a 59% increase in the second week of January 2018 from the USDM results.

Table 6 shows the mean DA values for all drought indices and categories from the two models, and Figure 14 shows the time series of DA values for two models and drought indices. Overall, the results of MSDI were the highest among the drought indices, and the abnormal drought category (D0) was the highest. The DA values of MSDI from the SWAT model were 64, 60, 47, 34, and 25% for all drought categories, and 62, 61, 48, 35, and 25% for the VIC model. Thus, the results of the MSDI implied that the MSDI was better than the other drought indices for forecasting purposes, and the performances of the two models were similar since the mean value of differences for all drought categories was less than 2%. Additionally, DA values for SSI were 42, 35, 16, 2, and 1% for the SWAT model and were 35, 27, 9, 2, and 0% for the VIC model. Finally, DA values for SBI were 25, 13, 6, 2, and 0% for the SWAT model and were 29, 22, 9, 2, and 0% for the VIC model. Thus, results of drought forecasting imply that the predictability of drought forecasting using only one variable (i.e., soil moisture and baseflow) was more uncertain than multiple variables.

The mean DA values of MSDI were the highest in the two models, and DA values decreased as the drought severity increased. These results imply that a drought index considered by one hydro-meteorological variable is more uncertain in forecasting drought conditions. Additionally, the disagreement rates of simulated drought conditions increase with increasing lead-time of the forecast (Figure 14), which would be closely associated with increasing meteorological uncertainty from CFSv2 with increasing lead time. [27] described the properties of the MSDI, and the MSDI was able to capture the drought onset comparable to the precipitation pattern and was able to capture drought persistence similar to the soil moisture, which implied the improved performance of drought monitoring compared to the SPI or SSI. Additionally, the MSDI showed advanced achievements in certain areas where the SPI or SSI did not properly represent the drought conditions. Thus, it can be

said that these properties of the MSDI also lead to better performances of drought forecasting with mitigating uncertainties.

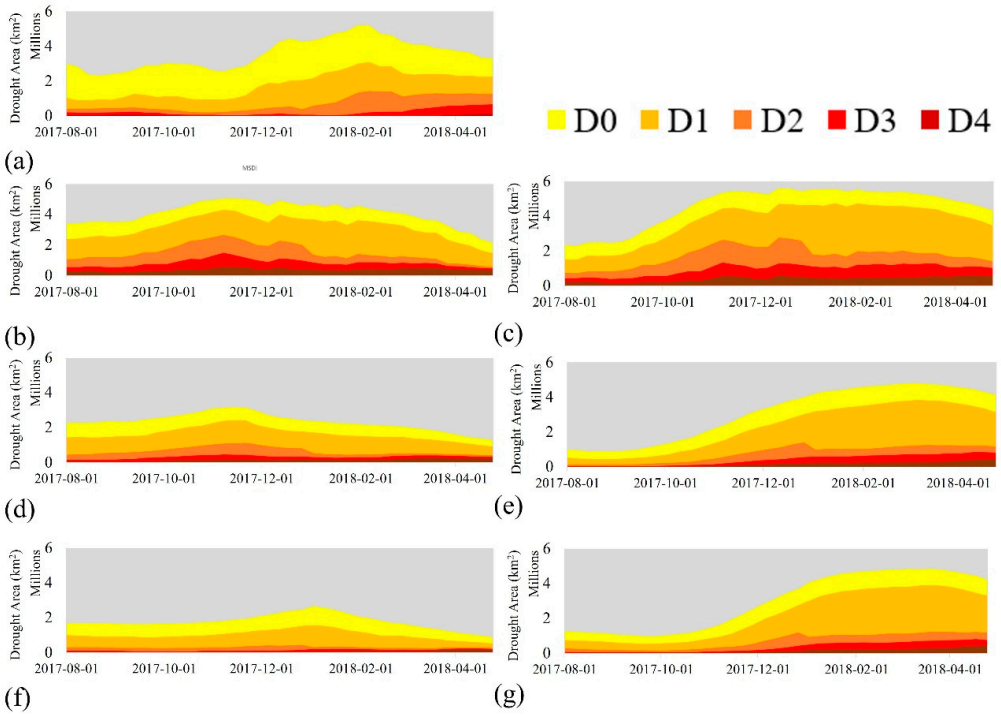

Figure 13. Weekly comparisons of drought areas of the USDM and drought indices computed from the VIC and SWAT models for the forecasting period. (**a**) Weekly drought categories from the USDM. (**b**) Weekly drought categories from the results of MSDI from the SWAT model. (**c**) Weekly drought categories from the results of MSDI from the VIC model. (**d**) Weekly drought categories from the results of SSI from the SWAT model. (**e**) Weekly drought categories from the results of SSI from the VIC model. (**f**) Weekly drought categories from the results of SBI from the SWAT model. (**g**) Weekly drought categories from the results of SBI from the VIC model.

Table 6. Mean DA values for drought indices and categories from the two models for the forecasting period between August 2017 and January 2018 (unit: %). Higher values indicate that the drought indices captured drought conditions better compared to USDM categories.

Model	Drought Indices	D0	D1	D2	D3	D4
SWAT	MSDI	64	60	47	34	25
	SSI	42	35	16	2	1
	SBI	25	13	6	2	0
VIC	MSDI	62	61	48	35	25
	SSI	35	27	9	2	0
	SBI	29	22	9	2	0

Figure 15 shows spatial maps and bar charts that indicate increases in precipitation and temperature uncertainty with increasing lead time. Figure 15a shows the spatial maps for grids where the absolute values of differences between monthly CPC observations and CFSv2 exceed 20 mm for the forecasting period (August 2017 to January 2018). If a value obtained by subtracting the CPC observation from CFSv2 is less than −20 mm, it is symbolized as red, and represents an underestimation of precipitation by CFSv2. However, if a value is more than 20 mm, it is displayed in green, and indicates an overestimation by CFSv2. Additionally, Figure 15b shows the total number of grids that exceed −20 or 20 mm for each month of the forecasting period. Figure 15c,d show the

results of monthly temperature with the same approach, but the exceedance level is 1 °C. As shown in Figures 15d and 16b, the total number of grids increased with lead time for both precipitation and temperature, which indicated increasing meteorological uncertainty from CFSv2. In addition, another possible uncertainty was the resolution of the CFSv2 dataset (0.937°) and the kriging interpolation because it downscaled 926 grids (0.937°) to 3275 grids (0.5°).

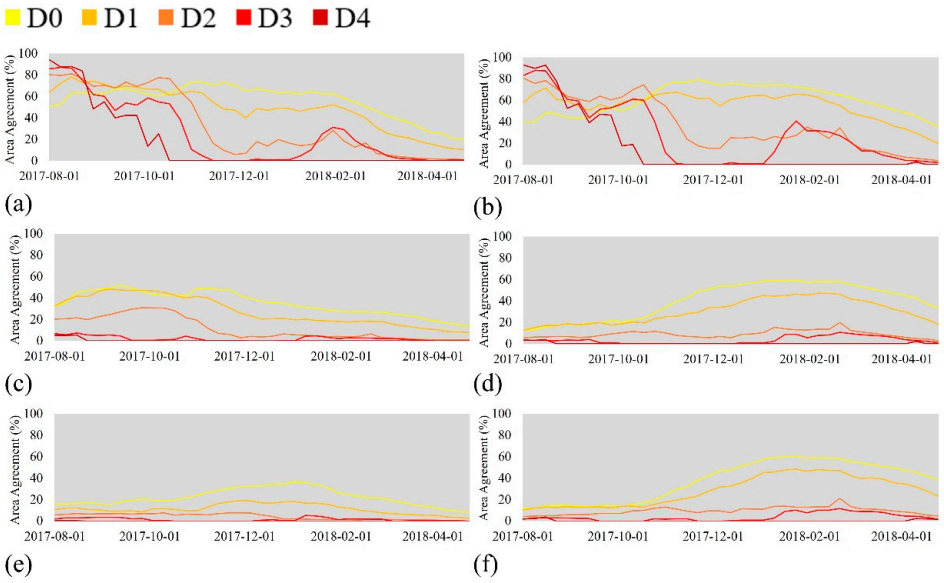

Figure 14. Weekly time series of drought agreement (DA) values of drought indices from the two models for the forecasting period (August 2017 to April 2018). The DA was calculated as a ratio of the intersected area to the total area of USDM (intersected area between USDM and drought indices/USDM). (**a**) Weekly time-series of DA from the results of MSDI from the SWAT model. (**b**) Weekly time-series of DA from the results of MSDI from the VIC model. (**c**) Weekly time-series of DA from the results of SSI from the SWAT model. (**d**) Weekly time-series of DA from the results of SSI from the VIC model. (**e**) Weekly time-series of DA from the results of SBI from the SWAT model. (**f**) Weekly time-series of DA from the results of SBI from the VIC model.

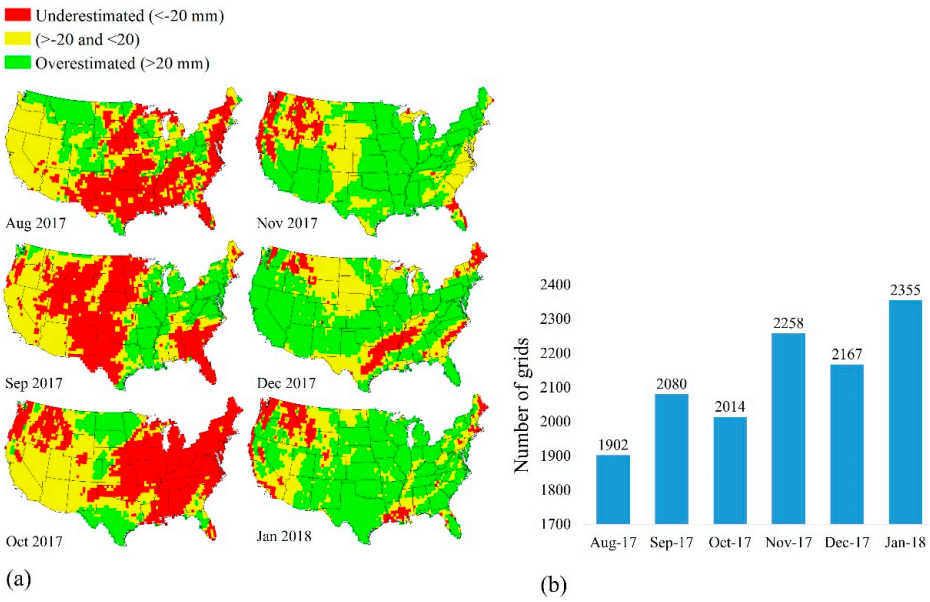

Figure 15. *Cont.*

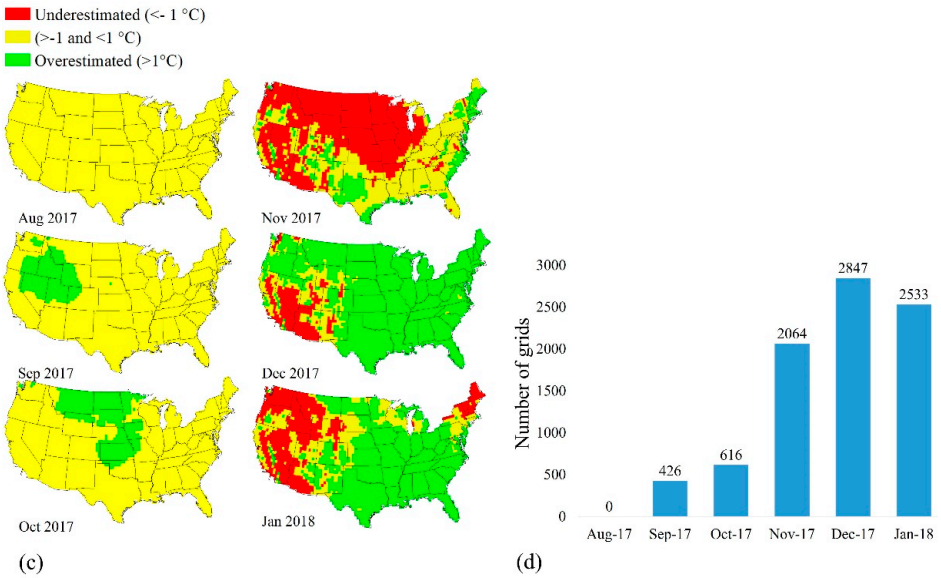

Figure 15. Spatial maps and bar charts for a number of grids where the absolute value of differences between monthly precipitation from CPC observations and CFSv2 exceed 20 mm, and monthly mean temperature exceed 1 °C. (**a**) Spatial maps for a number of grids where the absolute values of differences between monthly precipitation from CPC observation and CFSv2 exceed 20 mm. If a value obtained by subtracting the CPC observation from CFSv2 is less than −20 mm, it is symbolized as red and represents an underestimation compared to CFSv2. However, if the value is more than 20 mm, it is displayed in green and indicates an overestimation compared to CFSv2. Finally, if the value is between −20 and 20 mm, it is symbolized as yellow. (**b**) Total number of grids where the absolute values of monthly differences exceed 20 mm (**c**) Spatial maps for a number of grids where the absolute values of differences exceed 1 °C. If a value obtained by subtracting the CPC observation from CFSv2 is less than −1 °C, it is symbolized as red and represents an underestimation compared to CFSv2. However, if the value is more than 1 °C, it is displayed in green and indicates an overestimation compared to CFSv2. Finally, if the value is between −1 °C and 1 °C, it is symbolized as yellow. (**d**) Total number of grids where the absolute values of monthly differences exceed 1 °C for the forecasting period.

Figure 16 shows drought severity maps for the CONUS that indicate forecasted drought conditions from the drought indices from August 2017 to January 2018. During the first two months (August and September 2017) with the MSDI estimation, the mean values of DA for all drought categories were 68% and 63% for the SWAT and VIC models, respectively. Thus, it can be said that drought areas and all severities were relatively comparable with the USDM for the first two months. However, during the next two months (October and November 2017), the mean DA values were 42% and 43% for the SWAT and VIC models. Additionally, the mean DA values were 26% and 33% for the last two months (December 2017 to January 2018). More specifically, from November 2017 through January 2018, there were overestimations of predicted droughts (e.g., California, Oregon, and Washington) by the two models, and some of the actual drought conditions from the USDM were not captured by the two models (e.g., Arizona). These results also imply that simulating drought conditions with increasing lead-time of the forecast is dependent on the accuracy of temperature and precipitation forecasts derived from the climate models.

Additionally, an analysis of drought occurrence probabilities for the forecasting period was carried out. Figure S2 in the Supplementary Materials shows the comparisons of drought probability from the USDM, VIC-MSDI, and SWAT-MSDI. Due to the meteorological uncertainties from the CFSv2 (Figure 15), some drought areas were not captured by the MSDI estimations, and some drought areas were overestimated by the MSDI.

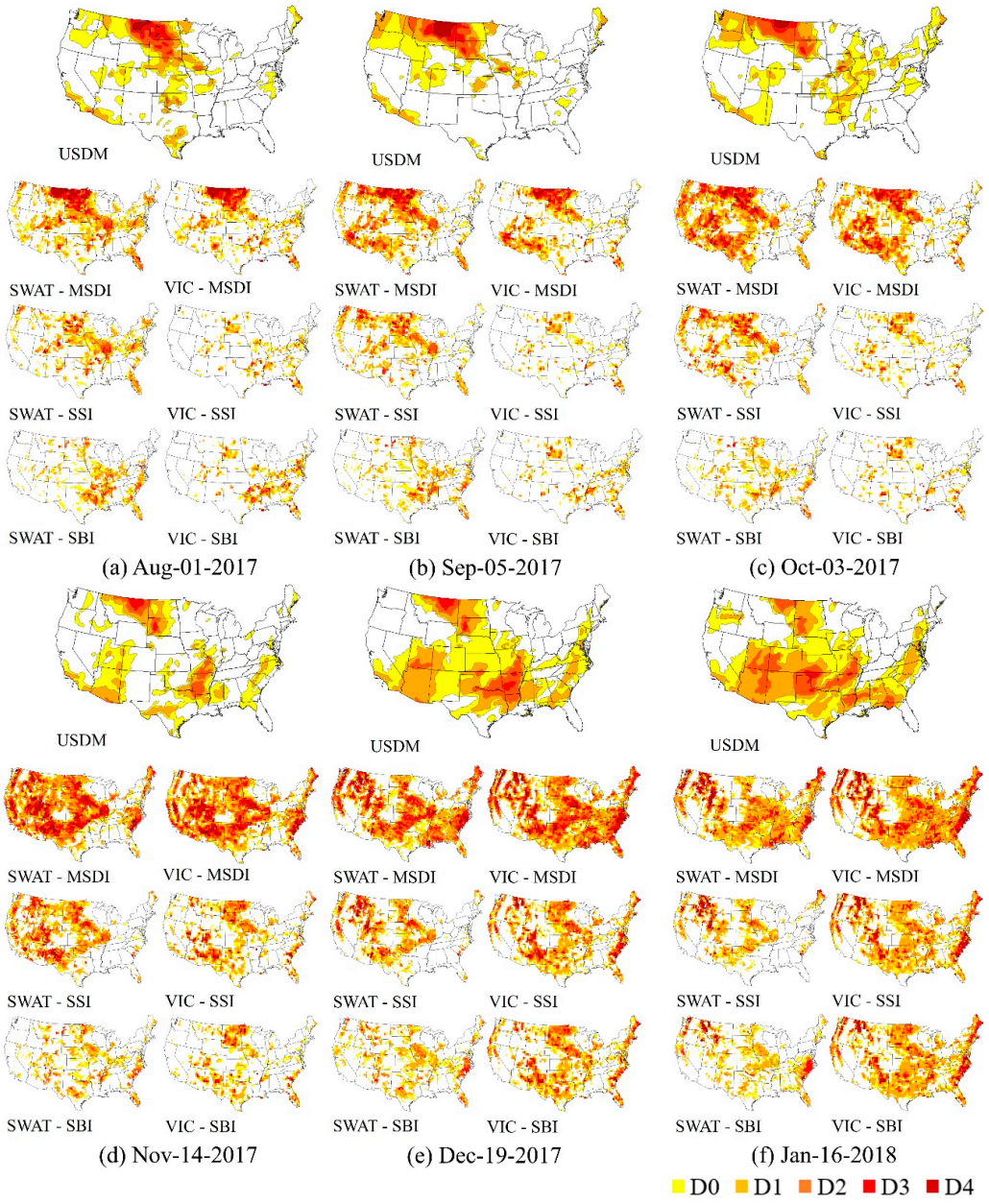

Figure 16. Spatial maps of drought conditions from the USDM and drought indices from the SWAT and VIC models for the forecasting period (August 2017 to April 2018). For the USDM, MSDI, SSI, and SBI maps, yellow to brown areas represent the five categories of drought conditions. (**a**) USDM and MSDIs for 1 August 2017. (**b**) USDM and MSDIs for 5 September 2017. (**c**) USDM and MSDIs for 3 October 2017. (**d**) USDM and MSDIs for 14 November 2017. (**e**) USDM and MSDIs for 19 December 2017. (**f**) USDM and MSDIs for 16 January 2018.

Finally, we carried out an analysis of the box and whisker charts for each category of the drought areas for the forecasting period (August 2017 to April 2018) (Figure S1 in the Supplementary Materials). As shown in Figure S1a–e, blues boxes indicate the results of the USDM drought categories, and other boxes indicate the results of drought indices from the SWAT and VIC models. The range of boxes from the MSDI closely overlapped with USDM for the D0 category, which showed the highest DA values during the forecasting period.

4. Conclusions

A reliable drought monitoring and forecasting framework is essential for water resource management and drought mitigation strategies. This study investigated a retrospective drought simulation and near-real-time drought forecasting method using simulated hydrometeorological variables using the SWAT and VIC models with CFSv2 for the CONUS. The retrospective analysis was performed for January 2012 to July 2017, and drought forecasting was performed for August 2017 through April 2018 with a weekly time step of drought indices. The accuracies of the retrospective and forecasting methods is evaluated by comparisons of the weekly USDM maps and simulated drought maps of drought indices for the CONUS region. The important findings of this study are as follows:

(1) For the retrospective period, the mean DA values were 63% and 66% for the MSDI simulation from the SWAT and VIC models and were 65% and 66% for SSI simulation (D0 category). In addition, the mean IA values were 70% and 72% for the MSDI simulation and were 71% and 72% for the SSI simulation (D0 category). The results imply that drought simulations with two models and multiple drought indices are useful in monitoring overall drought conditions for the CONUS.

(2) For the forecasting period, the mean DA values were 65% and 62% for the MSDI simulation for the SWAT and VIC models, which indicates that a forecast using the MSDI estimation in the SWAT and VIC models with CFSv2 is capable of reliable real-time drought forecasting. However, the mean DA values were 42% and 35% for the SSI estimation and were 25% and 29% for the SBI simulation from the SWAT and VIC models. Thus, an evaluation of drought forecasting using multiple hydrometeorological components (e.g., precipitation and soil moisture) from multiple hydrologic models would provide an advanced understanding of the characteristics of drought and would reduce uncertainties that arise from using only one model and variable.

(3) Drought forecasting by the MSDI estimation for two months of lead time was relatively reliable (68% and 63% for the SWAT and VIC models). However, drought forecasting with increasing lead-times would be associated with increasing meteorological uncertainty. Additionally, drought forecasting using only one variable (i.e., SSI and SBI) was not predictable even in the first two months (23% and 10% for SSI; 7% and 7% for SBI).

(4) The USDM is commonly conservative in judging an exceptional drought condition (D4), even though percentiles of soil moisture observation were less than 2% (D4 category). However, in the case of other drought categories (D0 to D3), some drought events predicted by the USDM commonly exceeded the results of soil moisture percentiles. Thus, these results would imply an underestimation of exceptional drought area monitoring from the USDM.

(5) For the results of retrospective and forecasting periods, the sources of uncertainties can be manifold; (a) USDM uses a more complicated method than the drought indices; (b) USDM may use other meteorological inputs, not just precipitation and temperature from CPC or CFSv2; (c) there are increasing meteorological uncertainties from CFSv2 with increasing lead time; and (d) the spatial resolutions of CFSv2 and CPC are different.

(6) The proposed method provides weekly drought maps, which is better than the current approach which only provides an overall, seasonal outlook on drought trends (e.g., CPC drought outlook). Additionally, weekly forecasting maps for the entire CONUS can contribute to water resource management, crop planning, drought risk management, and adopting drought mitigation strategies in advance.

Since the proposed approach has some uncertainties associated with estimating drought forecasting, combination with a remote sensing dataset (e.g., NDVI) and multiple climate indices (e.g., North Atlantic Oscillation) would provide a better assessment of drought forecasting in the future [74].

Supplementary Materials: The following are available online at http://www.mdpi.com/2071-1050/10/6/1799/s1, Figure S1: Box and whisker charts for each category of the drought areas. Each color of boxes represents the results of USDM and drought indices for the forecasting period (August 2017 to April 2018). The blue box shows the results of USDM, the green box represents SWAT-MSDI, orange boxes represent VIC-MSDI, the blue-green box represents SWAT-SSI, the brown box represents VIC-SSI, light green represents SWAT-SBI, and yellow box represents VIC-SBI. The upper and lower whiskers represent maximum and minimum values, first quartile represents 25%, median represents 50%, and third quartile represents 75% of the values. Figure S2: Spatial maps of drought probability for the USDM, VIC-MSDI, and SWAT-MSDI during the forecasting period (August 2017–April 2018). Yellow, orange, and red areas represent the higher drought probability, while green areas represent lower drought probability.

Author Contributions: Conceptualization, V.S. and H.K.; Methodology, V.S.; Software, H.K.; Validation, V.S., and H.K.; Formal Analysis, H.K.; Investigation, V.S. and H.K.; Resources, V.S.; Data Curation, V.S and H.K.; Writing—Original Draft Preparation, H.K.; Writing—Review and Editing, V.S.; Visualization, H.K; Supervision, V.S.; Project Administration, V.S.; Funding Acquisition, V.S.

Funding: This research received no external funding.

Acknowledgments: This project was funded, in part, by the Virginia Agricultural Experiment Station (Blacksburg) and the Hatch Program of the National Institute of Food and Agriculture, U.S Department of Agriculture (Washington, D.C.). We also thank Institute for Critical Technology and Applied Science (ICTAS), Graduate School at Virginia Tech for the graduate fellowship provided to the first author during his graduate education.

Conflicts of Interest: The authors declare no conflict of interest.

References

1. Sternberg, T. Regional drought has a global impact. *Nature* **2011**, *472*, 169. [CrossRef] [PubMed]
2. Sheffield, J.; Wood, E.F. *Drought: Past Problems and Future Scenarios*; Routledge: Abingdon-on-Thames, UK, 2012.
3. Changnon, S.A.; Pielke, R.A., Jr.; Changnon, D.; Sylves, R.T.; Pulwarty, R. Human factors explain the increased losses from weather and climate extremes. *Bull. Am. Meteorol. Soc.* **2000**, *81*, 437–442. [CrossRef]
4. Karl, T.R.; Gleason, B.E.; Menne, M.J.; McMahon, J.R.; Heim, R.R.; Brewer, M.J.; Kunkel, K.E.; Arndt, D.S.; Privette, J.L.; Bates, J.J.; et al. US temperature and drought: Recent anomalies and trends. *Eos Trans. Am. Geophys. Union* **2012**, *93*, 473–474. [CrossRef]
5. McEvoy, D.J. *Physically Based Evaporative Demand as a Drought Metric: Historical Analysis and Seasonal Prediction*; University of Nevada: Reno, NV, USA, 2015.
6. Clark, J.S.; Iverson, L.; Woodall, C.W.; Allen, C.D.; Bell, D.M.; Bragg, D.C.; D'amato, A.W.; Davis, F.W.; Hersh, M.H.; Ibanez, I.; et al. The impacts of increasing drought on forest dynamics, structure, and biodiversity in the United States. *Glob. Chang. Biol.* **2016**, *22*, 2329–2352. [CrossRef] [PubMed]
7. AghaKouchak, A. A baseline probabilistic drought forecasting framework using standardized soil moisture index: Application to the 2012 United States drought. *Hydrol. Earth Syst. Sci.* **2014**, *18*, 2485–2492. [CrossRef]
8. Hayes, M.; Svoboda, M.; Le Comte, D.; Redmond, K.T.; Pasteris, P. *Drought Monitoring: New Tools for the 21st Century*; Taylor and Francis: Abingdon, UK, 2005; pp. 53–69.
9. Steinemann, A.C. Using climate forecasts for drought management. *J. Appl. Meteorol. Climatol.* **2006**, *45*, 1353–1361. [CrossRef]
10. Luo, L.; Wood, E.F. Monitoring and predicting the 2007 US drought. *Geophys. Res. Lett.* **2007**, *34*. [CrossRef]
11. Yan, H.; Moradkhani, H.; Zarekarizi, M. A probabilistic drought forecasting framework: A combined dynamical and statistical approach. *J. Hydrol.* **2017**, *548*, 291–304. [CrossRef]
12. Ribeiro, A.; Pires, C.A. Seasonal drought predictability in Portugal using statistical-dynamical techniques. *J. Phys. Chem. Earth* **2016**, *94*, 155–166. [CrossRef]
13. Mishra, A.K.; Singh, V.P. A review of drought concepts. *J. Hydrol.* **2010**, *391*, 202–216. [CrossRef]
14. Halmstad, A.; Najafi, M.R.; Moradkhani, H. Analysis of precipitation extremes with the assessment of regional climate models over the Willamette River Basin, USA. *Hydrol. Process.* **2013**, *27*, 2579–2590. [CrossRef]
15. Niemeyer, S. New Drought Indices. *Water Manag.* **2008**, *80*, 267–274.
16. Kang, H.; Sridhar, V. Combined statistical and spatially distributed hydrological model for evaluating future drought indices in Virginia. *J. Hydrol. Reg. Stud.* **2017**, *12*, 253–272. [CrossRef]
17. Sehgal, V.; Sridhar, V. Effect of hydroclimatological teleconnections on the watershed-scale drought predictability in the southeastern United States. *Int. J. Climatol.* **2018**, *38*, e1139–e1157. [CrossRef]

18. Thilakarathne, M.; Sridhar, V. Characterization of future drought conditions in the Lower Mekong River Basin. *Weather Clim. Extrem.* **2017**, *17*, 47–58. [CrossRef]
19. Kang, H.; Sridhar, V. Assessment of Future Drought Conditions in the Chesapeake Bay Watershed. *JAWRA* **2018**, *54*, 160–183. [CrossRef]
20. McKee, T.B.; Doesken, N.J.; Kleist, J. Drought Monitoring with Multiple Time Series. In Proceedings of the 8th Conference on Applied Climatology, Anaheim, CA, USA, 17–22 January 1993.
21. Mishra, A.K.; Singh, V.P. Analysis of drought severity-area-frequency curves using a general circulation model and scenario uncertainty. *J. Geophys. Res. Atmos.* **2009**, *114*. [CrossRef]
22. Zargar, A.; Sadiq, R.; Naser, B.; Khan, F.I. A review of drought indices. *Environ. Rev.* **2011**, *19*, 333–349. [CrossRef]
23. Paulo, A.; Martins, D.; Pereira, L.S. Influence of precipitation changes on the SPI and related drought severity. An analysis using long-term data series. *Water Resour. Manag.* **2016**, *30*, 5737–5757. [CrossRef]
24. Belayneh, A.; Adamowski, J.; Khalil, B.; Ozga-Zielinski, B. Long-term SPI drought forecasting in the Awash River Basin in Ethiopia using wavelet neural network and wavelet support vector regression models. *J. Hydrol.* **2014**, *508*, 418–429. [CrossRef]
25. Bonaccorso, B.; Cancelliere, A.; Rossi, G. Probabilistic forecasting of drought class transitions in Sicily (Italy) using standardized precipitation index and North Atlantic oscillation index. *J. Hydrol.* **2015**, *526*, 136–150. [CrossRef]
26. Hao, Z.; AghaKouchak, A. Multivariate standardized drought index: A parametric multi-index model. *Adv. Water Resour.* **2013**, *57*, 12–18. [CrossRef]
27. Hao, Z.; AghaKouchak, A. A nonparametric multivariate multi-index drought monitoring framework. *J. Hydrometeorol.* **2014**, *15*, 89–101. [CrossRef]
28. Madadgar, S.; Moradkhani, H. A Bayesian framework for probabilistic seasonal drought forecasting. *J. Hydrometeorol.* **2013**, *14*, 1685–1705. [CrossRef]
29. Cancelliere, A.; Di Mauro, G.; Bonaccorso, B.; Rossi, G. Drought forecasting using the standardized precipitation index. *Water Resour. Manag.* **2007**, *21*, 801–819. [CrossRef]
30. Morid, S.; Smakhtin, V.; Bagherzadeh, K. Drought forecasting using artificial neural networks and time series of drought indices. *Int. J. Climatol.* **2007**, *27*, 2103–2111. [CrossRef]
31. Zhang, X.; Tang, Q.; Liu, X.; Leng, G.; Li, Z. Soil moisture drought monitoring and forecasting using satellite and climate model data over Southwestern China. *J. Hydrometeorol.* **2017**, *18*, 5–23. [CrossRef]
32. Sridhar, V.; Hubbard, K.G.; You, J.; Hunt, E. Development of soil moisture index to quantify agricultural drought and its 'user-friendliness' in severity-area-duration assessment. *J. Hydrometeor.* **2008**, *9*, 660–676. [CrossRef]
33. Sridhar, V.; Jaksa, W.T.A.; Fang, B.; Lakshmi, V.; Hubbard, K.G.; Jin, X. Evaluating bias corrected AMSR-E soil moisture using in-situ observations and model estimates. *Vadose Zone J.* **2013**. [CrossRef]
34. Liang, X.; Lettenmaier, D.P.; Wood, E.F.; Burges, S.J. A simple hydrologically based model of land surface water and energy fluxes for general circulation models. *J. Geophys. Res. Atmos.* **1994**, *99*, 14415–14428. [CrossRef]
35. Mishra, V.; Cherkauer, K.A.; Shukla, S. Assessment of drought due to historic climate variability and projected future climate change in the midwestern United States. *J. Hydrometeorol.* **2010**, *11*, 46–68. [CrossRef]
36. Arnold, J.G.; Srinivasan, R.; Muttiah, R.S.; Williams, J.R. Large area hydrologic modeling and assessment part I: Model development. *JAWRA* **1998**, *34*, 73–89. [CrossRef]
37. Narasimhan, B.; Srinivasan, R. Development and evaluation of Soil Moisture Deficit Index (SMDI) and Evapotranspiration Deficit Index (ETDI) for agricultural drought monitoring. *Agric. For. Meteorol.* **2005**, *133*, 69–88. [CrossRef]
38. Shukla, S.; Lettenmaier, D.P. Seasonal hydrologic prediction in the United States: Understanding the role of initial hydrologic conditions and seasonal climate forecast skill. *Hydrol. Earth Syst. Sci.* **2011**, *15*, 3529–3538. [CrossRef]
39. Hao, Z.; Singh, V.P.; Xia, Y. Seasonal drought prediction: Advances, challenges, and future prospects. *Rev. Geophys.* **2018**, *56*. [CrossRef]
40. Saha, S.; Moorthi, S.; Wu, X.; Wang, J.; Nadiga, S.; Tripp, P.; Behringer, D.; Hou, Y.T.; Chuang, H.Y.; Iredell, M.; et al. The NCEP climate forecast system version 2. *J. Clim.* **2014**, *27*, 2185–2208. [CrossRef]

41. Svoboda, M.; LeComte, D.; Hayes, M.; Heim, R.; Gleason, K.; Angel, J.; Rippey, B.; Tinker, R.; Palecki, M.; Stooksbury, D.; et al. The drought monitor. *Bull. Am. Meteorol. Soc.* **2002**, *83*, 1181–1190. [CrossRef]
42. Lorenz, D.J.; Otkin, J.A.; Svoboda, M.; Hain, C.R.; Anderson, M.C.; Zhong, Y. Predicting US Drought Monitor states using precipitation, soil moisture, and evapotranspiration anomalies. Part I: Development of a nondiscrete USDM index. *J. Hydrometeorol.* **2017**, *18*, 1943–1962. [CrossRef]
43. Smith, A.B.; Katz, R.W. US billion-dollar weather and climate disasters: Data sources, trends, accuracy and biases. *Nat. Hazards* **2013**, *67*, 387–410. [CrossRef]
44. DHS. *National Preparedness Report*; U.S. Department. of Homeland Security: Washington, DC, USA, 2015; pp. 1–87.
45. Rippey, B.R. The US drought of 2012. *Weather Clim. Extrem.* **2015**, *10*, 57–64. [CrossRef]
46. Robeson, S.M. Revisiting the recent California drought as an extreme value. *Geophys. Res. Lett.* **2015**, *42*, 6771–6779. [CrossRef]
47. Wang, A.; Bohn, T.J.; Mahanama, S.P.; Koster, R.D.; Lettenmaier, D.P. Multimodel ensemble reconstruction of drought over the continental United States. *J. Clim.* **2009**, *22*, 2694–2712. [CrossRef]
48. Shukla, S.; Safeeq, M.; AghaKouchak, A.; Guan, K.; Funk, C. Temperature impacts on the water year 2014 drought in California. *Geophys. Res. Lett.* **2015**, *42*, 4384–4393. [CrossRef]
49. Mao, Y.; Nijssen, B.; Lettenmaier, D.P. Is climate change implicated in the 2013–2014 California drought? A hydrologic perspective. *Geophys. Res. Lett.* **2015**, *42*, 2805–2813. [CrossRef]
50. Wood, E.F.; Chaney, N.; Sheffield, J.; Yuan, X. Development of an Experimental African Drought Monitoring and Seasonal Forecasting System: A First Step Towards a Global Drought Information System. In *AGU Fall Meeting Abstracts*; American Geophysical Union: Washington, DC, USA, 2012.
51. Sheffield, J.; Wood, E.F.; Chaney, N.; Guan, K.; Sadri, S.; Yuan, X.; Olang, L.; Amani, A.; Ali, A.; Demuth, S.; et al. A drought monitoring and forecasting system for sub-Sahara African water resources and food security. *Bull. Am. Meteorol. Soc.* **2014**, *95*, 861–882. [CrossRef]
52. Chen, M.; Shi, W.; Xie, P.; Silva, V.; Kousky, V.E.; Wayne Higgins, R.; Janowiak, J.E. Assessing objective techniques for gauge-based analyses of global daily precipitation. *J. Geophys. Res. Atmos.* **2008**, *113*. [CrossRef]
53. Xie, P.; Chen, M.; Shi, W. CPC Unified Gauge-Based Analysis of Global Daily Precipitation. In Proceedings of the 24th Conference on Hydrology, Atlanta, GA, USA, 18 January 2010; Volume 2; in preprints.
54. Guttman, N.B. Accepting the standardized precipitation index: A calculation algorithm. *JAWRA* **1999**, *35*, 311–322. [CrossRef]
55. Nijssen, B.; O'donnell, G.M.; Hamlet, A.F.; Lettenmaier, D.P. Hydrologic sensitivity of global rivers to climate change. *Clim. Chang.* **2001**, *50*, 143–175. [CrossRef]
56. Nijssen, B.; O'Donnell, G.M.; Lettenmaier, D.P.; Lohmann, D.; Wood, E.F. Predicting the discharge of global rivers. *J. Clim.* **2001**, *14*, 3307–3323. [CrossRef]
57. Neitsch, S.L.; Arnold, J.G.; Kiniry, J.R.; Williams, J.R. *Soil and Water Assessment Tool Theoretical Documentation Version 2009*; Texas Water Resources Institute: College Station, TX, USA, 2011.
58. Arnold, J.G.; Moriasi, D.N.; Gassman, P.W.; Abbaspour, K.C.; White, M.J.; Srinivasan, R.; Santhi, C.; Harmel, R.D.; Van Griensven, A.; Van Liew, M.W.; et al. SWAT: Model use, calibration, and validation. *Trans. ASABE* **2012**, *55*, 1491–1508. [CrossRef]
59. Wang, D.; Hejazi, M.; Cai, X.; Valocchi, A.J. Climate change impact on meteorological, agricultural, and hydrological drought in central Illinois. *Water Resour. Res.* **2011**, *47*. [CrossRef]
60. Ashraf Vaghefi, S.; Mousavi, S.J.; Abbaspour, K.C.; Srinivasan, R.; Yang, H. Analyses of the impact of climate change on water resources components, drought and wheat yield in semiarid regions: Karkheh River Basin in Iran. *Hydrol. Process.* **2014**, *28*, 2018–2032. [CrossRef]
61. Ahn, S.R.; Jeong, J.H.; Kim, S.J. Assessing drought threats to agricultural water supplies under climate change by combining the SWAT and MODSIM models for the Geum River basin, South Korea. *Hydrol. Sci. J.* **2016**, *61*, 2740–2753. [CrossRef]
62. Trambauer, P.; Maskey, S.; Winsemius, H.; Werner, M.; Uhlenbrook, S. A review of continental scale hydrological models and their suitability for drought forecasting in (sub-Saharan) Africa. *Phys. Chem. Earth Parts A/B/C* **2013**, *66*, 16–26. [CrossRef]
63. Jones, C.B. *Geographical Information Systems and Computer Cartography*; Addison Wesley Longman: Harlow, UK, 1997.

64. USDA (U.S. Department of Agriculture). *Soil Conservation Service, National Engineering Handbook, Hydrology (Section 4, Chapters 4–10)*; GPO: Washington, DC, USA, 1972.
65. Homer, C.; Huang, C.; Yang, L.; Wylie, B.; Coan, M. Development of a 2001 national land-cover database for the United States. *Photogramm. Eng. Remote Sens.* **2004**, *70*, 829–840. [CrossRef]
66. Griffin, D.; Anchukaitis, K.J. How unusual is the 2012–2014 California drought? *Geophys. Res. Lett.* **2014**, *41*, 9017–9023. [CrossRef]
67. Livneh, B.; Hoerling, M.P. The physics of drought in the US Central Great Plains. *J. Clim.* **2016**, *29*, 6783–6804. [CrossRef]
68. Griffies, S.M.; Harrison, M.J.; Pacanowski, R.C.; Rosati, A. A technical guide to MOM4. GFDL Ocean Group Technical Report No. 5. *Geophys. Fluid Dyn. Lab.* **2004**, *5*, 371.
69. AghaKouchak, A. A multivariate approach for persistence-based drought prediction: Application to the 2010–2011 East Africa drought. *J. Hydrol.* **2015**, *526*, 127–135. [CrossRef]
70. Gringorten, I.I. A plotting rule for extreme probability paper. *J. Geophys. Res.* **1963**, *68*, 813–814. [CrossRef]
71. Benestad, R.E.; Haugen, J.E. On complex extremes: Flood hazards and combined high spring-time precipitation and temperature in Norway. *Clim. Chang.* **2007**, *85*, 381–406. [CrossRef]
72. Wood, E.F.; Lettenmaier, D.P.; Zartarian, V.G. A land-surface hydrology parameterization with subgrid variability for general circulation models. *J. Geophys. Res. Atmos.* **1992**, *97*, 2717–2728. [CrossRef]
73. Boughton, W.C. A review of the USDA SCS curve number method. *Soil Res.* **1989**, *27*, 511–523. [CrossRef]
74. Marj, A.F.; Meijerink, A.M. Agricultural drought forecasting using satellite images, climate indices and artificial neural network. *Int. J. Remote Sens.* **2011**, *32*, 9707–9719. [CrossRef]